Renormalization Groups and Condensed Matter

David R. Nelson, Grace H. Zhang

August 8, 2023

Contents

Statistical mechanics of freely fluctuating elastic sheets

5

In the previous chapter, we studied the physics of one-dimensional chain polymers. In this section, we'll be studying two-dimensional sheet polymers. In particular, we'll focus on the interesting physics that arises when they're allowed to freely fluctuate, such as when in a vacuum or a good solvent. One example of a freely-fluctuating sheet polymer is the spectrin polymer skeleton of a red blood cell. The red blood cell has a biconcave shape, no nuclei, and its membrane consists of a lipid bilayer lined underneath with the spectrin skeleton, which can be extracted from the RBC and studied experimentally [85]. Another example is freestanding graphene. While graphene is populated with electrons described by a band structure with Dirac cones in momentum space [86], freely fluctuating graphene also has quite interesting mechanical properties.

The theoretical framework can be described as follows. Imagine a reference elastic sheet that's flat at zero temperature. When the sheet is thermally excited at finite temperatures, it may crumple, much like the linear polymer chains we studied in the previous section. However, even if the sheet doesn't crumple, it can still wrinkle and fluctuate in interesting ways, leading to profound changes in its mechanical strength. We will now derive a description of this physics in terms of a nonlinear strain tensor. As shown in Figure 5.1, if we track a short reference line segment $d\vec{r}_0$ as we begin to distort the sheet, the image of that line segment $d\vec{r}$ will typically get longer or shorter due to local undulations or some partial crumpling. This new image segment that gets mapped from the reference segment into some slightly distorted object is described by

$$\vec{r}(x_1, x_2) = \vec{r}_0 + \begin{pmatrix} f(x_1, x_2) \\ u_1(x_1, x_2) \\ u_2(x_1, x_2) \end{pmatrix} \tag{5.1}$$

which is the flat reference state $\vec{r}_0$ plus two in-plane displacements u_1, u_2 and out-of-plane (flexural) displacement f, and where $0 \leq x_1, x_2, \leq L$ are the internal coordinates (imagine a warped piece of graph paper) that allow us to traverse the sheet. The squared length $d^2 r$ associated with Eq. 5.1 can then be written as,

$$dr^2 = dr_0^2 + 2u_{\alpha\beta} dx_\alpha dx_\beta \tag{5.2}$$

where the stretching (strain) tensor $u_{\alpha\beta}$ is nonlinear in the out of plane displacement field $f(x_1, x_2)$,

$$u_{\alpha\beta}(\vec{x}) = \frac{1}{2} \left[\frac{\partial u_\alpha(\vec{x})}{\partial x_\beta} + \frac{\partial u_\beta(\vec{x})}{\partial x_\alpha} + \frac{\partial f}{\partial x_\alpha} \frac{\partial f}{\partial x_\beta} \right]. \tag{5.3}$$

We can derive Eqs. 5.2 and 5.3 via a long-wavelength description applicable to any elastic solid, including metals, insulators, wherever you can blur your eyes and coarse-grain over the microscopic lattice structure. On the long length scales, the normal modes of the displacements (f, u_1, u_2) would describe, for example, in-plane acoustic longitudinal and transverse phonons as well as flexural phonons in a thin
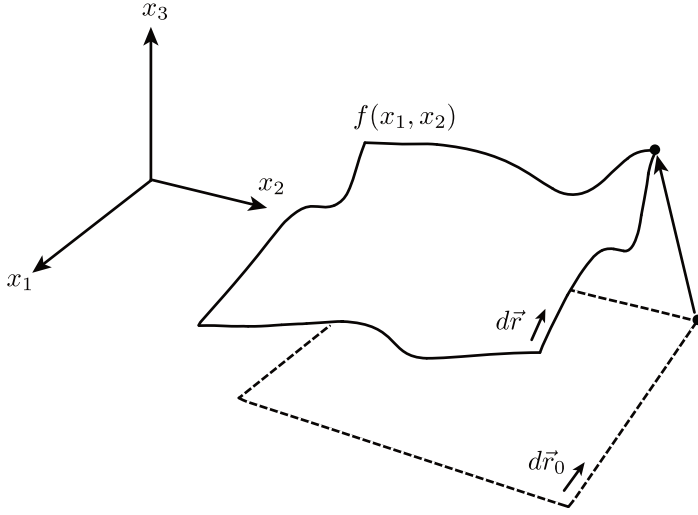
Figure 5.1: The flat reference state $\vec{r}_0(x_1, x_2)$ and the possible crumpled actual state $\vec{r}(x_1, x_2)$ of a sheet polymer, as a function of the reference state in-plane coordinates (x_1, x_2) that allow us to traverse the sheet. The changes a segment in the flat state dr_0 undergoes as it is mapped to the actual state gives us the stretching tensor of the actual system.

elastic membrane. Just as in the Debye theory of the specific heat of crystals, one can quantify these phonon fields at low temperatures [86], although this will not be our primary concern in this chapter.

To make contact with other chapters of this book, we'll take an unconventional approach and derive the stretching tensor from a Landau theory, starting in the high temperature crumpled phase of a sheet polymer. We can then study this problem by doing a Landau expansion in the (soft) tangents to the surface, which are the order parameters for this problem, similar to the linear polymer tangents employed in Chapter 4,

$$\vec{t}_\alpha = \frac{\partial \vec{r}(x_1, x_2)}{\partial x_\alpha}, \quad \alpha = 1, 2. \tag{5.4}$$

If we coarse-grain over multiple ripples, these tangents are not required to be unit vectors, since they can be stretched or compressed by short wavelength undulations. Once we drop below a potential critical temperature T_c, we can then study the properties of a possible broken-symmetry flat phase. Of course, Landau theory is a mean field theory, so we'll have to incorporate fluctuations and check if the physics is changed by the Hohenberg-Mermin-Wager Goldstone modes invoked by the Hohenberg-Mermin-Wagner theorem.

5.1 Statistical mechanics of sheet polymers

We assume the probability of a particular sheet polymer configuration will depend on the Boltzmann factor associated with some coarse-grained Landau free energy,

$$\sim e^{-F[\vec{r}(x_1, x_2)]/k_B T}. \tag{5.5}$$

To calculate statistical mechanical averages, we'll be doing functional integrals over all the possible $\vec{r}(x_1, x_2)$ configurations. Note that $\vec{r}$ is a three-dimensional vector field and $\underset{\sim}{x} \equiv (x_1, x_2)$ represents two-dimensional internal coordinates. We'll be using $\vec{}$ to denote three-dimensional vectors and $\underset{\sim}{}$ to denote two-dimensional vectors.

Henceforth, $D = 2$ will denote the internal space and $d = 3$ will denote the embedding space. To get the free energy F, we'll expand in tangents, up to quartic order, in analogy to what we could do for the linear polymer chains of Chapter 4 in scales large compared to the persistence length [87],

$$F[\vec{r}(x_1, x_2)] = \int d^2x \left[\frac{1}{2}\tilde{\kappa}(\partial_\alpha^2 \vec{r})^2 + \frac{1}{2}a(\partial_\alpha \vec{r})^2 + b(\partial_\alpha \vec{r} \cdot \partial_\beta \vec{r})^2 + c\left(\sum_\gamma \vec{t}_\gamma \cdot \vec{t}_\gamma\right)^2 \right], \quad (5.6)$$

where we have adopted the Einstein summation convention. The form of the Landau potential is determined by translational and rotational invariance; in the absence of edge forces, there are no terms odd in $\vec{t}$ because that would indicate a preferred direction. Note the following

1. The first term in Eq. 5.6 gives rise to a bending energy proportional to spatial variations of the membrane tangents, $\int d^2x \sum_{\alpha\beta}(\partial_\alpha \vec{t}_\beta)^2$, measuring how fast the tangents turn/bend as we move along the undulating surface of the sheet polymer. This term will be especially important in the crumpled phase, where the magnitudes of the undulations are large.
2. Polynomial terms in the tangents $\{\vec{t}_\alpha\}$ include

$$\frac{a}{2}\sum_{\alpha=1}^2 |\vec{t}_\alpha|^2 + b\sum_{\alpha,\beta}(\vec{t}_\alpha \cdot \vec{t}_\beta)^2 + c\left(\sum_\gamma \vec{t}_\gamma \cdot \vec{t}_\gamma\right)^2 \quad (5.7)$$

where there are two distinct quartic coupling coefficients $b, c > 0$, both positive such that the free energy is stable when the tangents are large, and $a = a'(T - T_c)$ where T_c is the crumpling temperature, signified by a change of sign in a at the transition.
3. For any configuration $\vec{r}(x_1, x_2)$, the free energy F is invariant under both translations and rotations of $\vec{r}$

$$\vec{r}(x_1, x_2) \to \vec{r}_0 + \vec{r}(x_1, x_2), \quad \vec{r}(x_1, x_2) \to \mathcal{R}(\hat{n}, \theta)\vec{r}(x_1, x_2). \quad (5.8)$$

where $\mathcal{R}(\hat{n}, \theta)$ is a three-dimensional rotation matrix about the $\hat{n}$-axis with angle θ.
4. F is also invariant under rotations of the *internal* coordinates (x_1, x_2):

$$\begin{pmatrix} x_1 \\ x_2 \end{pmatrix} \to \mathcal{R}(\phi)\begin{pmatrix} x_1 \\ x_2 \end{pmatrix} = \begin{pmatrix} x_1' \\ x_2' \end{pmatrix}, \quad \mathcal{R}(\phi) = \begin{pmatrix} \cos\phi & \sin\phi \\ -\sin\phi & \cos\phi \end{pmatrix} \quad (5.9)$$

Eventually, we'll carry out functional integrals to do statistical mechanics with F, but for now, we can obtain an approximate understanding by just minimizing the free energy using a saddle point approximation, which may be a reasonable description at low temperatures. Within mean field theory, we can assume negative $a < 0$ ($T < T_c$) and minimize the free energy functional in Eq. 5.6 with the following ansatz

$$\vec{r}_0(x_1, x_2) \equiv m[x_1\vec{e}_1 + x_2\vec{e}_2], \quad (5.10)$$

where $\vec{e}_1$ and $\vec{e}_2$ are orthogonal unit vectors on the tangent plane of a reference sheet. The order parameter magnitude m is nonzero in the flat phase and measures the spatial extent of the sheet polymer despite shrinkage due to thermal fluctuations. (At $T = 0$, when we neglect quantum fluctuations, we expect $m = L$ for an $L \times L$ square

reference sheet.) The two order parameters are the tangents

$$\{\vec{t}_1, \vec{t}_2\} = m\{\vec{e}_1, \vec{e}_2\}. \tag{5.11}$$

On substituting the linear ansatz in Eq. 5.10 into the free energy in Eq. 5.6, the first term (bending energy) vanishes. The tangent magnitude m corresponding to the minimum energy configuration, left as an exercise to this reader, is given by

$$m = \frac{1}{2}\sqrt{\frac{-a}{b+2c}}. \tag{5.12}$$

Note that this Landau theory predicts that the order parameter magnitude m scales as follows

$$m \sim \sqrt{-a} \sim (T_c - T)^{1/2} \tag{5.13}$$

as the crumpling transition is approached from below.

5.1.1 Connection with a metric tensor

Our Landau free energy measures a penalty for how much the metric tensor deviates from that of a flat sheet. For $T < T_c$, it is helpful to rewrite the free energy by completing the square,

$$F = \text{const.} + \int d^2x \left[\frac{1}{2}\tilde{\kappa} \left(\partial_\alpha^2 r\right)^2 + b \left(\frac{\partial \vec{r}}{\partial x_\alpha} \cdot \frac{\partial \vec{r}}{\partial x_\beta} - m^2 \delta_{\alpha\beta}\right)^2 + c \left(\frac{\partial \vec{r}}{\partial x_\gamma} \cdot \frac{\partial \vec{r}}{\partial x_\gamma} - 2m^2\right)^2 \right] \tag{5.14}$$

where $m^2 = \frac{1}{4}\frac{-a}{b+2c} > 0$. The energy is controlled by a tangent bending energy proportional to $\tilde{\kappa}$, and two stretching terms proportional to elastic constants b and c, which control the energy cost associated with deviations from an idealized flat "preferred metric":

$$d\vec{r}(x_1, x_2) = \frac{\partial \vec{r}}{\partial x_1}dx_1 + \frac{\partial \vec{r}}{\partial x_2}dx_2 \tag{5.15}$$

$$d^2s \equiv |d\vec{r}(x_1, x_2)|^2 = \sum_{\alpha\beta}\left(\frac{\partial \vec{r}}{\partial x_\alpha} \cdot \frac{\partial \vec{r}}{\partial x_\beta}\right) dx_\alpha dx_\beta \equiv g_{\alpha\beta}dx_\alpha dx_\beta. \tag{5.16}$$

The fluctuating metric tensor associated with a particular sheet polymer configuration can then be read off as

$$g_{\alpha\beta} = \frac{\partial \vec{r}}{\partial x_\alpha} \cdot \frac{\partial \vec{r}}{\partial x_\beta}, \tag{5.17}$$

which describes how distances warp and change in the system, while the preferred metric that minimizes Eq. 5.14 is

$$g^0_{\alpha\beta} = m^2 \delta_{\alpha\beta}. \tag{5.18}$$

5.1.2 Goldstone modes of the flat phase

Similar to our dicussion of linear polymer chains on scales below the persistence length (see Chapter 4), the free energy landscape described by Eq. 5.14 has the shape of a wine bottle. Hence, we expect to find Goldstone modes in the flat phase of the sheet polymer. We can derive these Goldstone phonon modes by parametrizing an elastic membrane with small deviations from flatness as,

$$\vec{r}(x_1, x_2) \approx m[x_1 + u_1(x_1, x_2)]\vec{e}_1 + m[x_2 + u_2(x_1, x_2)]\vec{e}_2 + mf(x_1, x_2)\vec{e}_3, \quad \vec{e}_3 = \vec{e}_1 \times \vec{e}_2 \tag{5.19}$$

where $u_1(x_1, x_2)$ and $u_2(x_1, x_2)$ are the in-plane phonon displacements and the field $f(x_1, x_2)$ describes the flexural (out-of-plane) phonons.

We now substitute this ansatz into the free energy in Eq. 5.14 and determine the energetic cost (bending, stretching) associated with deviation from the idealized mean field theory metric at long wavelengths. The distorted metric tensor associated with Eq. 5.19 is now

$$g_{\alpha\beta} = \frac{\partial \vec{r}}{\partial x_\alpha} \cdot \frac{\partial \vec{r}}{\partial x_\beta} = m^2 \left[\delta_{\alpha\beta} + 2u_{\alpha\beta} \right], \tag{5.20}$$

where the second term on the RHS describes the distortion due to fluctuations in the sheet polymer. The strain matrix $u_{\alpha\beta}$ representing these distortions is given by

$$u_{\alpha\beta} = \frac{1}{2} \left(\frac{\partial u_\alpha}{\partial x_\beta} + \frac{\partial u_\beta}{\partial x_\alpha} \right) + \frac{1}{2} \frac{\partial f}{\partial x_\alpha} \frac{\partial f}{\partial x_\beta} + O(\partial_\alpha u_\beta)^2. \tag{5.21}$$

The first part of the strain tensor consists of the symmetrized derivatives of the in-plane phonon fields, which show up in studies of flat two-dimensional crystals, e.g. a continuum theory of the specific heat, where (as in a Debye theory) phonon modes should be quantized at low temperatures. Anti-symmetric contributions do not appear because derivative combinations such as

$$\Omega_{\alpha\beta} = \frac{1}{2} \left(\partial_\alpha u_\beta - \partial_\beta u_\alpha \right) \tag{5.22}$$

are not rotationally invariant. The terms second order in ∂u can be neglected relative to $\partial_\alpha u_\beta$ terms, but an extra term second order in $\partial_\alpha f$ is kept because it is the lowest order term in f. The new physics due to flexural phonons comes entirely from this term. One can approximate the bending energy term in the Landau free energy in a similar fashion,

$$\left(\frac{\partial^2 \vec{r}}{\partial x_\beta^2} \right)^2 = m^2 \left(\nabla^2 f \right)^2 + O \left[\frac{\partial^2 f}{\partial x_\alpha^2} \frac{\partial^2 u_\beta}{\partial x_\gamma^2} \right], \tag{5.23}$$

which, like the metric in Eq. 5.20, is also proportional to m^2. Thus, up to an additive constant, the free energy can be expressed as

$$F = \frac{\kappa}{2} \int d^2x (\nabla^2 f)^2 + \int d^2x \left[\mu u_{\alpha\beta}^2 + \frac{\lambda}{2} u_{\gamma\gamma}^2 \right], \tag{5.24}$$

where the (nonlinear) strain tensor is given by Eq. 5.21. The first term describes

the bending energy, and the remainder of the RHS consists of elastic terms of two-dimensional elastic sheet that one finds in standard elasticity textbooks [88], known since the 19th century. The coupling coefficient of the tangent derivatives $\tilde{\kappa}$ gives rise to the bending rigidity κ while the quartic couplings b and c from Landau theory gave rise to the Lamé coefficients μ and λ,

$$\kappa = m^2 \tilde{\kappa}, \quad \mu = m^2 b, \quad \lambda = m^2 c. \tag{5.25}$$

Note that, since $m \sim (T_c - T)^{1/2}$, these quantities vanish linearly as the crumpling temperature is approached from below.

5.1.3 Analogy with superconductivity

There is an interesting analogy between elasticity theory and the Ginzburg-Landau model of superconductivity in a low temperature limit originally studied by Fritz and Heinz London [89]. This phenomenalogical model was written down for a charged superfluid, where electron pairs give rise to a complex order parameter $\psi(\vec{x})$ wave function. Gradients of the order parameter are coupled minimally to a vector potential $\vec{A}$, which fluctuates in a superconductor, leading to a magnetic field energy proportional to $|\vec{\nabla} \times \vec{A}|^2$ in the total free energy,

$$F_{GL} = \int d^2x \left[\frac{1}{2m} \left| \left(\frac{\hbar}{i} \vec{\nabla} - \frac{e}{c} \vec{A} \right) \psi(\vec{x}) \right|^2 + \frac{r}{2} |\psi|^2 + u|\psi|^4 + \frac{1}{8\pi} |\vec{\nabla} \times \vec{A}|^2 \right] \tag{5.26}$$

Upon going down to low temperatures, where $r \approx a(T - T_c) < 0$, we can minimize the free energy to get the preferred amplitude of the order parameter $\psi_0 = \sqrt{-r/4u}$. On substituting $\psi(\vec{r}) = \psi_0 e^{i\theta(\vec{r})}$ into the free energy functional, we recover the London model of low-energy excitations in superconductors, which typically works well for $0 < T \ll T_c$,

$$F_{GL} = \text{const.} + \int d^2x \left[\frac{1}{2} K |\vec{\nabla}\theta - \frac{e}{\hbar c}\vec{A}|^2 + \frac{1}{8\pi} \left(\vec{\nabla} \times \vec{A} \right)^2 \right], \quad K = |\psi_0|^2 \frac{\hbar^2}{m} \tag{5.27}$$

The form of this free energy is quite similar to Eq. 5.24, describing the low energy excitations of the sheet polymers (see Table 5.1). The gradients of the in-plane phonon field in Eq. 5.21 are like the gradients of the phase angle for the superconductor. The nonlinear portion of the strain tensor is in fact like a matrix vector potential $A_{ij} = -\frac{1}{2}(\partial_i f)(\partial_j f)$. There's something quite subtle going on in both of these problems. In the superconductivity problem, after determining the preferred magnitude of $\psi(\vec{r})$ from mean field theory, the leftover degree of freedom is a *single* scalar phase variable $\theta(\vec{r})$, from which we subtract the vector potential $\vec{A}$ that in general has *two* degrees of freedom. For a given a vector potential $\vec{A}$, the free energy in Eq. 5.27 can achieve minimal energy if the first term $\sim |\vec{\nabla}\theta - \frac{e}{\hbar c}\vec{A}|^2$ can be made to disappear. However, if $\vec{A}$ has a nonzero curl, as happens when a magnetic field is present, there does not exist in general a single-valued function $\theta(\vec{r})$ such that $\vec{\nabla}\theta = \frac{e}{\hbar c}\vec{A}$, which would minimize the first gradient term in Eq. 5.27. In other words, one can't in general cancel out an independently fluctuating variable with two degrees of freedom with just a single component phase field. This superconducting analog of geometrical frustration gives rise to vortices arrayed in an Abrikosov flux lattice when there's an external magnetic field applied to type II superconductors [90].

	Superconductor	Fluctuating sheet polymer
Goldstone modes	$\theta(x)$	$\vec{u}(x) = [u_1(x), u_2(x)]$ (in-plane phonons)
Stiffness	$K = m\|\psi_0\|^2 \frac{\hbar^2}{m^2}$	μ, λ (Lamé coefficients)
Vector potential	$\vec{A}(x)$	$A_{ij} = -\frac{1}{2}\frac{\partial f}{\partial x_\alpha}\frac{\partial f}{\partial x_\beta}$
Magnetic field	$\vec{B} = \vec{\nabla} \times \vec{A}$	$\det\left(\frac{\partial^2 f}{\partial x_\alpha \partial x_\beta}\right)$ (Gaussian curvature)
	Linear field theory	Nonlinear field theory

Table 5.1: A comparison of the analogous quantities in the problems of superconductivity and two-dimensional elastic sheets.
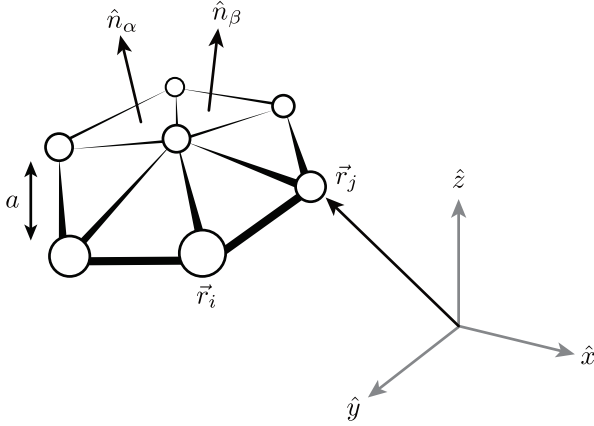
Figure 5.2: Microscopic model of elasticity on a sheet polymer with monomer spacing a, accounting for both surface stretching and surface bending energies.

In the problem of the sheet polymer, the nonlinear flexural phonon term plays the role of a *matrix* vector potential $A_{\alpha\beta}(x) = \frac{1}{2}\partial_\alpha f(x)\partial_\beta f(x)$. We can ask again, is it possible to make the strain tensor vanish $u_{\alpha\beta} = 0$ to minimize the energy in Eq. 5.24? Now, there are two in-plane phonon degrees of freedom associated with $\partial_\beta u_\alpha + \partial_\alpha u_\beta$, but the symmetric vector-potential-like quantity $A_{\alpha\beta}(x)$ has 3 degrees of freedom, so these two contributions cannot in general cancel out. A measure of the frustration in the Ginzburg-Landau theory of superconductivity is the curl of the vector potential $\vec{\nabla} \times \vec{A}$. The analogous quantity in the theory of sheet polymers turns out to be the determinant of $\partial_\alpha\partial_\beta f$, which is precisely the Gaussian curvature of an elastic membrane [5, 67]. When these quantities are nonzero (e.g. elastic membranes with curvature or superconductors in a magnetic field), the corresponding problems become more intricate and harder to solve. The analogy between these two problems is summarized in Table Table 5.1. The analogy is not perfect, because there is only an approximate mapping of the bending energy in Eq. 5.24 onto the field energy $\sim |\vec{\nabla} \times \vec{A}|^2$ of a superconductor.

5.1.4 Simulation model

A simple microscopic model is often used to simulate and test some of these continuum ideas that we'll be studying in the forthcoming sections. The idea is to triangulate the surface of some material into a discrete lattice (if the mesh is fine enough, its long-wavelength behavior should be the same as that in continuum system). We can then connect each pair of neighboring sites on this lattice with permanent spring-like bonds. This permanent connectivity will leave out defects, flows, and liquid-like

behavior, but is not a bad approximation to a coarse-grained sheet polymer, such as graphene. One can then assign normal unit vectors $\hat{n}$ to each triangular plaquette (i.e. the plane defined by three neighboring lattice points, see Figure 5.2), which gives us another way to parameterize bending energy. The microscopic Hamiltonian is then [79]

$$H = -\kappa \sum_{\langle \alpha\beta \rangle} \hat{n}_\alpha \cdot \hat{n}_\beta + \sum_{\langle ij \rangle} V(|\vec{r}_i - \vec{r}_j|), \tag{5.28}$$

where here, $\langle \alpha\beta \rangle$ indexes neighboring plaquettes of the triangulated sheet and $\langle ij \rangle$ indexes the neighboring vertices. The normals $\hat{n}$ can be thought of as a proxy for classical Heisenberg spins living on a two dimensional sheet. The positions of the mass points define a triangular lattice that is dual to the honeycomb lattice defined by the $\hat{n}$ (this triangular lattice can be regarded as a discrete approximation to the honeycomb lattice of graphene). Nearest neighbor mass points also interact with each other via a pair interaction $V(r)$, e.g. the Lenard-Jones potential,

$$V(r) = 4\epsilon \left[\left(\frac{\sigma}{r}\right)^{12} - \left(\frac{\sigma}{r}\right)^{6} \right], \tag{5.29}$$

equivalent for small displacements to springs with repulsive excluded volume interactions. We will assume that the bonds do not break (on the time scale of room temperature experiments of e.g. free standing graphene, this is certainly true), and replace the interaction $V(r)$ in Eq. 5.29 by a simple parabolic form

$$V(r_{ij}) \approx \frac{1}{2}k[r_{ij} - a]^2, \quad r_{ij} = |\vec{r}_i - \vec{r}_j|, \tag{5.30}$$

where a is the equilibrium length of the bond between two neighboring sites at $T = 0$. Monte Carlo and molecular dynamics simulations using this model have yielded many insights over the years.

5.1.5 Low temperature statistical mechanics of the flat phase

To fix the basic ideas, we briefly recapitulate elementary aspects of the model we have set up for the statistical mechanics of two-dimensional sheet polymers. At low temperatures, we assume a strain-free configuration such that $u_{ij} = 0$. Minimizing the bending term in the free energy in Eq. 5.6 (with a summation convention on α),

$$\frac{\kappa}{2} \int d^2x \left(\frac{d^2\vec{r}}{dx_\alpha^2}\right)^2, \tag{5.31}$$

then gives us the flat state of the sheet

$$\vec{r}_0 = x_1\vec{e}_1 + x_2\vec{e}_2, \quad 0 \le x_1, x_2 \le L, \tag{5.32}$$

where we can set the order parameter magnitude $m \approx 1$ in Eq. 5.10 at low temperatures. Let us again consider deviations from a flat state spanned by $\vec{e}_1$ and $\vec{e}_2$, with $\vec{e}_i \cdot \vec{e}_j = \delta_{ij}$, specifically the energy cost of deformations from both in-plane and out-of-plane

stretching of the sheet polymer

$$\vec{r}(x_1, x_2) \;\;=\;\; \vec{r}_0(x_1, x_2) + \begin{pmatrix} u_1(x_1, x_2) \\ u_2(x_1, x_2) \\ f(x_1, x_2) \end{pmatrix} \tag{5.33}$$

$$= \;\; (x_1 + u_1)\vec{e}_1 + (x_2 + u_2)\vec{e}_2 + f\vec{e}_3, \tag{5.34}$$

where we have used Eq. 5.32 and $\vec{e}_3 = \vec{e}_1 \times \vec{e}_2$ is normal to the flat state at $T = 0$. Note that Eq. 5.32 assumes a broken rotational symmetry, with a preferred normal direction given by $\hat{e}_3$. It remains to be seen if this flat state is stable to the low energy excitations that give rise to the Hohenberg-Mermin-Wagner theorem in related two-dimensional systems!

We can now calculate the stretching in a small reference line element

$$d\vec{r}_0 = \begin{pmatrix} dx_1 \\ dx_2 \\ 0 \end{pmatrix}, \quad d\vec{r} = \begin{pmatrix} (1 + \partial_1 u_1)dx_1 + (\partial_2 u_1)dx_2 \\ (\partial_1 u_2)dx_1 + (1 + \partial_2 u_2)dx_2 \\ (\partial_1 f)dx_1 + (\partial_2 f)dx_2 \end{pmatrix}. \tag{5.35}$$

Because the line element $d\vec{r}_0$ is typically stretched or compressed when mapped onto $d\vec{r}$, the energy will increase. The stretching is described by the squared length

$$ds^2 = |d\vec{r}|^2 = d^2 r + 2u_{\alpha\beta}dx_\alpha dx_\beta \tag{5.36}$$

where the strain tensor $u_{\alpha\beta}$ is

$$u_{\alpha\beta} = \frac{1}{2}(\partial_\alpha u_\beta + \partial_\beta u_\alpha) + \frac{1}{2}(\partial_\alpha f)(\partial_\beta f) + O\left[\frac{1}{2}(\partial_\alpha u_\gamma)(\partial_\beta u_\gamma)\right]. \tag{5.37}$$

The free energy of a nearly flat sheet polymer is thus composed of a bending energy and a stretching energy,

$$F[f, u] = \frac{1}{2}\kappa \int d^2 x (\nabla^2 f)^2 + \frac{1}{2} \int d^2 x \left[2\mu u_{\alpha\beta}^2 + \lambda u_{\gamma\gamma}^2\right], \tag{5.38}$$

where κ is the bending rigidity and λ, μ are the Lamé elastic coefficients. the first term describes the bending energy

$$\frac{\kappa}{2} \int d^2 x \left[\partial_1^2 \vec{r} + \partial_2^2 \vec{r}\right]^2 \tag{5.39}$$

which has a "soft" energetic penalty ($\sim q^4 |\vec{r}_{\vec{q}}|^2$ in Fourier space) that keeps the polymer approximately flat. The second term is the stretching energy quadratic in the strain tensor, made up of two distinct terms one can make out of a 2 by 2 strain tensor that are invariant to rotations of the coordinates: u_{kk}^2 (tracing over the strain tensor and then squaring it), and u_{ij}^2 (squaring the strain tensor and then tracing it). Note that the trace operation for a matrix A is invariant to rotations $\mathcal{R}$ of the coordinates $\text{tr}(\mathcal{R}A\mathcal{R}^{-1}) = \text{tr}(\mathcal{R}^{-1}\mathcal{R}A) = \text{tr}(A)$. As mentioned previously, the strain matrix is frustrated (i.e. nonzero): given a flexural phonon configuration $f(x_1, x_2)$, since we can't in general cancel the 3-component matrix $A_{ij} = \frac{1}{2}(\partial_i f)(\partial_j f)$ with two in-plane phonon fields (u_1, u_2).

In the following sections, we'll study this model in two limits:

1. $\kappa \to \infty$: This allows us to set the out-of-plane f field to 0, making the sheet

polymer flat with only in-plane elastic distortions.

2. $\mu, \lambda \to 0$: This might sound like a strange thing to do, but it in fact describes liquid membranes (e.g. lipid bilayers, which are the primary components of animal cell membranes).

5.2 In-plane elasticity of flat sheet polymers

When $\kappa \to \infty$, bending is too costly, so we can set the out-of-plane gradients of the sheet to $\partial_\alpha f = 0$. The free energy is then,

$$F_0 = \frac{1}{2} \int d^2x \left[2\mu u_{\alpha\beta}^2 + \lambda u_{\gamma\gamma}^2 \right], \quad u_{\alpha\beta} = \frac{1}{2} \left(\partial_\alpha u_\beta + \partial_\beta u_\alpha \right) \tag{5.40}$$

where the strain tensor is now linear in the sheet displacement fields. We can study the phonon modes in this system by going to Fourier space, being careful to treat the finite momentum $q > 0$ and zero momentum $q = 0$ degrees of freedom separately. As we'll show, there are 2 normal modes for $q \neq 0$ distortions and 3 normal modes for $q = 0$ distortions.

5.2.1 Case I: finite momentum modes

Let ρ be the areal mass density of the sheet polymer. If we take a small part of the sheet and locally distort it away from its ground state with in-plane phonon displacements, there will be a restoring force leading to the following equation of motion,

$$\rho \frac{\partial^2 \underset{\sim}{u}(\underset{\sim}{x}, t)}{\partial t^2} = -\frac{\delta F_0}{\delta \underset{\sim}{u}(\underset{\sim}{x}, t)} = \mu \nabla^2 \underset{\sim}{u} + (\mu + \lambda) \underset{\sim}{\nabla}(\underset{\sim}{\nabla} \cdot \underset{\sim}{u}) \tag{5.41}$$

which is a wave equation that exhibits both transverse and longitudinal sound modes, and underscore tildes again indicate two-dimensional vectors in the three-dimensional embedding space.

The longitudinal sound (compressional) displacements are parallel to the phonon displacements ($\underset{\sim}{q} \parallel \underset{\sim}{u}$), and are described by,

$$u_\alpha(\underset{\sim}{x}, t) = u_L \hat{q}_\alpha e^{i \underset{\sim}{q} \cdot \underset{\sim}{x} - i\omega_L t}, \tag{5.42}$$

where u_L is a constant amplitude and $\omega_L = \omega_L(q)$ is the characteristic frequency of the longitudinal sound with the following dispersion relation (as can be checked from Eq. 5.41),

$$\omega_L(\underset{\sim}{q}) = \sqrt{\frac{2\mu + \lambda}{\rho}} |\underset{\sim}{q}|. \tag{5.43}$$

The transverse sound displacements, perpendicular to phonon wavevector $\underset{\sim}{q}$, are

$$u_\alpha = u_T \left(\hat{z} \times \hat{q}_\alpha \right) e^{i \underset{\sim}{q} \cdot \underset{\sim}{x} - i\omega_T t}. \tag{5.44}$$

where u_T is a constant shear amplitude and the dispersion relation for $\omega_T = \omega_T(q)$ following from Eq. 5.41 is given by

$$\omega_T(q) = \sqrt{\frac{\mu}{\rho}}|q|. \tag{5.45}$$

The above results are quite familiar from standard 2d continuum elasticity theory dating back to the 19th century. We will now write them in a useful alternate way, using longitudinal and transverse projection operators. On going to Fourier space in two dimensions

$$u(x) = \frac{1}{L^2} \sum_q u(q) e^{iq \cdot x}, \tag{5.46}$$

the free energy can be expressed as a quadratic form for every wave vector q,

$$F_0 = \int \frac{d^2q}{(2\pi)^2} u_\alpha^*(q) G_{\alpha\beta}(q) u_\beta(q), \tag{5.47}$$

where $G_{\alpha\beta}(q)$ is the matrix phonon Green's function, expressed in terms of the projection operators as

$$G_{\alpha\beta}(q) = \mu q^2 \underbrace{\left(\delta_{\alpha\beta} - \frac{q_\alpha q_\beta}{q^2}\right)}_{P^T_{\alpha\beta}(q)} + (2\mu + \lambda)q^2 \underbrace{\frac{q_\alpha q_\beta}{q^2}}_{P^L_{\alpha\beta}(q)}. \tag{5.48}$$

Recall the important properties of the projection operators

$$P_T^2 = P_T, \quad P_L^2 = P_L, \quad P_T P_L = 0, P_L + P_T = 1, \tag{5.49}$$

which allow us to invert the phonon Green's function just by inspection

$$G_{\alpha\beta}^{-1}(q) = \frac{1}{\mu q^2}\left(\delta_{\alpha\beta} - \frac{q_\alpha q_\beta}{q^2}\right) + \frac{1}{(2\mu + \lambda)q^2}\frac{q_\alpha q_\beta}{q^2}. \tag{5.50}$$

5.2.2 Case II: zero momentum modes

We can separate out the zero-momentum component in the Fourier expansion of the strain tensor (somewhat like the separation used to treat Bose-Einstein condensation [91]),

$$u_{\alpha\beta}(x) = u_{\alpha\beta}^0 + \frac{1}{L^2} \sum_{q \neq 0} \frac{i}{2} \left[q_\alpha u_\beta(q) + q_\beta u_\alpha(q)\right] e^{iq \cdot x}. \tag{5.51}$$

The symmetric uniform field $u_{\alpha\beta}^0$ corresponding to $q = 0$ describes homogeneous long wavelength stretching and shearing of the elastic sheet, and has three degrees of freedom, while the second term for $q \neq 0$ has two degrees of freedom. How will this separation play out? There are many precedents in physics for separating out the $q = 0$ and $q \neq 0$ modes. We can take the infinite volume limit at the end and sometimes, the distinction matters, while other times, it does not. In this case, for the statistical mechanics of elastic sheets, we do have to be careful at $q = 0$ and allow 3 degrees of freedom instead of 2.
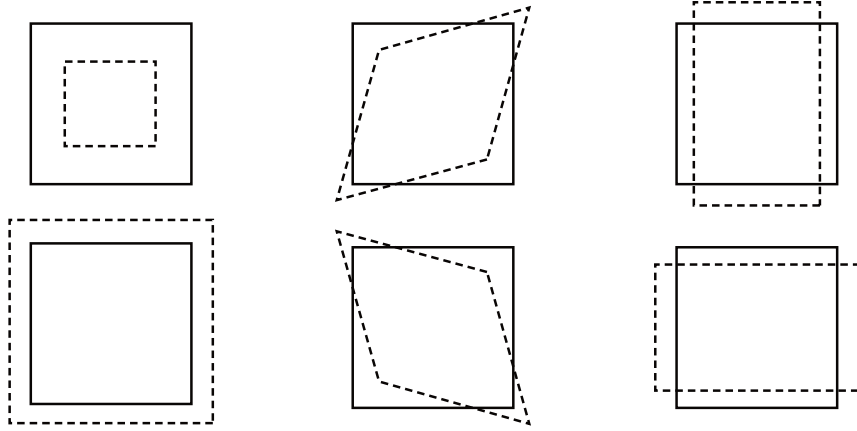
Figure 5.3: The three modes of uniform strain: dilation/compression, diagonal shear, and vertical/horizontal shear.

The in-plane displacement field corresponding to the first of the three zero-momentum modes shown in Figure 5.3 is

$$\underset{\sim}{u}(\underset{\sim}{x}) = \frac{1}{2}a\underset{\sim}{x}, \tag{5.52}$$

which describes a uniform dilation if $a > 0$ (and a compression if $a < 0$). The corresponding strain matrix is

$$u^0_{\alpha\beta} = \frac{1}{2}\left(\partial_\alpha u_\beta + \partial_\beta u_\alpha\right) = \begin{pmatrix} \frac{a}{2} & 0 \\ 0 & \frac{a}{2} \end{pmatrix}. \tag{5.53}$$

The free energy of the dilation corresponding to Eq. 5.40 is thus proportional to the area $\sim L^2$ and the dilation magnitude squared α^2

$$F_{\text{dilation}} = \frac{1}{2}(\mu + \lambda)a^2 L^2, \tag{5.54}$$

where $\mu + \lambda$ is the two-dimensional bulk modulus.

The second $q = 0$ normal mode describes diagonal shearings,

$$\begin{pmatrix} u_1(\underset{\sim}{x}) \\ u_2(\underset{\sim}{x}) \end{pmatrix} = \frac{1}{2}b\begin{pmatrix} x_2 \\ x_1 \end{pmatrix}, \quad u^0_{ij} = \begin{pmatrix} 0 & b/2 \\ b/2 & 0 \end{pmatrix} \tag{5.55}$$

and the shearing energy is

$$F_S = \frac{1}{2}\mu b^2 L^2, \tag{5.56}$$

where μ is the shear modulus.

Finally, the third mode describes vertical/horizontal shearing

$$\begin{pmatrix} u_1(\underset{\sim}{x}) \\ u_2(\underset{\sim}{x}) \end{pmatrix} = \frac{1}{2}\gamma\begin{pmatrix} x_1 \\ -x_2 \end{pmatrix}, \quad u^0_{\alpha\beta} = \begin{pmatrix} \gamma/2 & 0 \\ 0 & -\gamma/2. \end{pmatrix} \tag{5.57}$$

with energy

$$F_V = \frac{1}{2}\mu\gamma^2 L^2.$$
(5.58)

Note that the strain matrices for both the diagonal and the vertical shearing modes are traceless.

These three modes are summarized in Figure 5.3. The most general zero momentum strain matrix we can write then has three independent components, a, b, γ,

$$u^0_{\alpha\beta} = \frac{1}{2}\begin{pmatrix} a+\gamma & b \\ b & a-\gamma \end{pmatrix}.$$
(5.59)

which makes sense since $u_{\alpha\beta}$ is a symmetric 2 by 2 matrix. (We leave the reader to check that a rigid rotation leads to an antisymmetric component of the strain matrix and hence costs zero elastic energy.)

5.2.3 Response of planar crystals to external forces

Forces applied to the edge of a planar sheet polymer can be understood by looking at the edge normals, which also live in the plane. When projected along the normals, the forces applied at the edge are the work done to move the displacement field at the surface by u_i. If $\hat{m}(x)$ is the normal at the boundary of a 2d planar crystal, the resulting energy is

$$F_0 = \frac{1}{2}\int d^2x \left[2\mu u^2_{\alpha\beta} + \lambda u^2_\gamma\right] - \oint dx\hat{m}_\alpha\sigma_{\alpha\beta}u_\beta,$$
(5.60)

where $\sigma_{\alpha\beta}$ is the stress tensor acting on the edge, such that $\hat{m}_\alpha\sigma_{\alpha\beta} \equiv f_\beta$ is the β-th component of force acting on a direction perpendicular to the sheet normal $\hat{m}_\alpha$.

A stress tensor that produces a pure shear deformation is

$$\sigma_{\alpha\beta} = \sigma_0\begin{pmatrix} 0 & 1 \\ 1 & 0 \end{pmatrix},$$
(5.61)

while an elongational deformation is produced by

$$\sigma_{\alpha\beta} = \sigma_0\begin{pmatrix} 1 & 0 \\ 0 & 0 \end{pmatrix}.$$
(5.62)

Equation 5.61 represents tangential forces σ_0 applied to the top and bottom of a square elastic sheet (see Figure 5.4), while Eq. 5.62 describes pulling/elongating the solid along the $\hat{x}$ direction with a force σ_0. When you pull on an elastic solid, it typically elongates in the direction you're pulling and shrinks in the perpendicular

direction. How much it elongates along the direction pulled is determined by the Young's modulus Y. How much it shrinks is determined by the Poisson's ratio ν. In a similar fashion (as we shall see below), the displacements under the shear forces in Eq. 5.61 are determined by the shear modulus μ.

Upon converting the line integral in Eq. 5.60 into an area integral, we obtain

$$F_0 = \frac{1}{2} \int d^2x \left[2\mu u_{\alpha\beta}^2 + \lambda u_{\gamma\gamma}^2 - 2u_{\alpha\beta}\sigma_{\alpha\beta} \right]. \tag{5.63}$$

Let $\sigma_{xx} = \sigma_0$ be the stress corresponding to elongation in the $\hat{x}$-direction and $u_{\alpha\beta} = \bar{u}_{\alpha\beta}$ be the symmetric linear uniform strain tensor in $d = 2$ with three independent components,

$$\bar{u}_{\alpha\beta} = \begin{pmatrix} \bar{u}_{xx} & \bar{u}_{xy} \\ \bar{u}_{xy} & \bar{u}_{yy} \end{pmatrix}. \tag{5.64}$$

Upon minimizing the free energy in Eq. 5.63, we find the three independent strain components to be

$$\bar{u}_{xy} = 0, \quad \bar{u}_{xx} = \sigma_0/Y, \quad \bar{u}_{yy} = -\nu\bar{u}_{xx}, \tag{5.65}$$

where $\nu = \lambda/(\lambda + 2\mu)$ is the two-dimensional Poisson ratio and Y is the Young's modulus

$$Y = \frac{4\mu(\mu + \lambda)}{2\mu + \lambda}. \tag{5.66}$$

Here, $\bar{u}_{xx}$ describes the relative elongation of the undeformed sheet length L_x along $\hat{x}$,

$$L'_x = (1 + \bar{u}_{xx})L_x \quad \Rightarrow \quad \frac{\delta L_x}{L} = \bar{u}_{xx}, \tag{5.67}$$

while $\bar{u}_{yy}$ describes the relative shrinkage along $\hat{y}$,

$$L'_y = (1 + \bar{u}_{yy})L_y \quad \Rightarrow \quad \frac{\delta L_y}{L} = u_{yy} = -\nu\frac{\delta L_x}{L}. \tag{5.68}$$

Note that the Poisson ratio ν is typically positive (object shrinks in one direction when you pull on it in the transverse direction), but can also be negative for some special materials called auxetics (when you pull on the material in one direction, it *expands* in the transverse direction). For a simple example of auxetic behavior, try pulling on a wrinkled but approximately flat piece of paper: when you pull on one direction, it releases stored projected area to expand in the other direction!

If we insert the shear stress in Eq. 5.61 to Eq. 5.63, we find (for an $L \times L$ elastic square),

$$\frac{F}{L^2} = \left(\mu + \frac{1}{2}\lambda\right)\left(\bar{u}_{xx}^2 + \bar{u}_{yy}^2\right) + \lambda\bar{u}_{xx}\bar{u}_{yy} + 2\mu\bar{u}_{xy}^2 - 2\sigma_0\bar{u}_{xy}, \tag{5.69}$$

which is minimized when $\bar{u}_{xx} = \bar{u}_{yy} = 0$, and

$$\bar{u}_{xy} = \frac{\sigma_0}{2\mu}, \tag{5.70}$$

which defines the shear modulus μ.

5.3 Pure out-of-plane elasticity: "liquid" sheets (e.g. lipid bilayers)

Having discussed the limiting cases of perfectly flat membranes in the limit $\kappa \to \infty$, we now discuss membranes which bend but have liquid-like in-plane elasticity. We can think of sheet polymers with out-of-plane fluctuations in the $\mu, \lambda \to 0$ limit as liquid sheets, where the in-plane phonon displacements have zero cost such that atoms, as in a liquid, can wander around freely in response to forces. When these in-plane strains are eliminated, we're left with is the bending energy

$$F_0 = \frac{1}{2}\kappa \int d^2x (\nabla^2 f)^2. \tag{5.71}$$

and the membrane now resists only out-of-plane displacements

$$\vec{r}(x_1, x_2) = \begin{pmatrix} x_1 \\ x_2 \\ f(x_1, x_2) \end{pmatrix}, \tag{5.72}$$

with the local tangents being

$$\vec{t}_1 = \frac{\partial \vec{r}}{\partial x_1} = \begin{pmatrix} 1 \\ 0 \\ \frac{\partial f}{\partial x_1} \end{pmatrix}, \quad \vec{t}_2 = \frac{\partial \vec{r}}{\partial x_2} = \begin{pmatrix} 0 \\ 1 \\ \frac{\partial f}{\partial x_2} \end{pmatrix}. \tag{5.73}$$

In other words, even for a liquid sheet, out of plane fluctuations are resisted, since they incur an important bending energy cost. A good example is the lipid bilayer wall surrounding all animal cells, which is typically in a 2d liquid phase (see Figure 5.5).

For a liquid membrane whose reference state is in the xy-plane, the unit surface normal in three dimensions is given by

$$\hat{n}(x_1, x_2) \equiv \frac{\vec{t}_1 \times \vec{t}_2}{|\vec{t}_2 \times \vec{t}_2|} = \frac{1}{\sqrt{1 + |\nabla f|^2}} \begin{pmatrix} -\frac{\partial f}{\partial x_1} \\ -\frac{\partial f}{\partial x_2} \\ 1 \end{pmatrix} \tag{5.74}$$

On assuming spontaneous broken symmetry and long range order in the normals of the liquid membrane, the excitations about the ground state, analogous to spin waves in low-temperature magnets, are then undulations of the normals about its preferred direction. The thermally averaged component of the normal $\hat{n}(\underset{\sim}{x})$ along the $\hat{z}$-direction, given by

$$\langle \hat{n} \cdot \vec{e}_3 \rangle = \langle \cos \theta \rangle = \left\langle \frac{1}{\sqrt{1 + |\nabla f|^2}} \right\rangle \approx \langle 1 - \frac{\theta^2}{2} \rangle \approx \langle 1 - \frac{1}{2}|\nabla f|^2 \rangle, \tag{5.75}$$

must be close to 1 at low temperatures, where θ is the angle of $\hat{n}$ relative to $\hat{z}$.
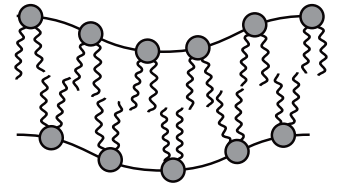
Figure 5.5: Schematic of a phospholipid bilayer, comprising the membrane of animal cells. The constituent molecules have polar, hydrophilic head groups, and hydrocarbon, hydrophobic tails.

Fluctuations in the tilt angle are thus controlled by

$$\langle \theta^2(\underset{\sim}{x}) \rangle = \langle |\nabla f|^2 \rangle = \int \frac{d^2q}{(2\pi)^2} q^2 \langle |f(q)|^2 \rangle \tag{5.76}$$

The bending free energy in Eq. 5.71 can be written in terms of Fourier components as,

$$F_0 = \frac{\kappa}{2} \int \frac{d^2q}{(2\pi)^2} q^4 |f_q|^2. \tag{5.77}$$

Upon applying the equipartition theorem $\langle |f(q)|^2 \rangle = \frac{k_B T}{\kappa q^4}$, Eq. 5.76 becomes,

$$\langle \theta^2(\underset{\sim}{x}) \rangle = \frac{k_B T}{\kappa} \int \frac{d^2q}{(2\pi)^2} \frac{1}{q^2} \sim \frac{k_B T}{\kappa} \ln\left(\frac{L}{a}\right), \tag{5.78}$$

which diverges logarithmically with system size.

Thus, the normals for these liquid sheets fluctuate much like the spins of a classical 3-component Heisenberg model in two dimensions! We find a logarithmic divergence in the tilt angle fluctuations for this two-dimensional problem upon assuming continuous broken symmetry in the direction of the normal. So for a big enough system, long range order is impossible for $2d$ liquid membranes, destroyed by thermal tilt angle undulations, much like the Hohenberg-Mermin-Wagner theorem applied to Heisenberg spins.

You may ask, how can a red blood cell surrounded by a lipid bilayer exist if long range order cannot persist in two-dimensional liquid membranes? If you work out the persistence length associated with the divergence in Eq. 5.78 i.e. the size such that $\langle \theta^2(\underset{\sim}{x}) \rangle \approx \pi/2$, you would get, using lipid bilayer bending rigidities, $\ell_p \approx 80\mu m$, a size much larger than the size of the red blood ($\approx 5\mu m$). So although these undulations are important for these red blood cells (they flicker when viewed under a light microscope), they're not enough to crumple in a way similar to a very long linear polymer. This physical argument does place an upper limit on how big a stable red blood cell with a given bending rigidity can be.

5.4 General treatment

Having studied the $\kappa \to \infty$ and $\mu, \lambda \to 0$ limits, we now return to the full expression for the free energy of a nearly flat sheet polymer,

$$F[f, u] = \frac{1}{2}\kappa \int d^2x (\nabla^2 f)^2 + \frac{1}{2} \int d^2x \left[2\mu u_{\alpha\beta}^2 + \lambda u_{\gamma\gamma}^2 \right] \tag{5.79}$$

with the nonlinear strain tensor u_{ij} given as usual by,

$$u_{\alpha\beta} = \frac{1}{2}(\partial_\alpha u_\beta + \partial_\beta u_\alpha) + \frac{1}{2}(\partial_\alpha f)(\partial_\beta f). \tag{5.80}$$

Note that the nonlinearity in the strain tensor only comes about when we allow the sheet to go into the third dimension. This problem, with three elastic constants, is actually similar to a massless field theory right at the critical point. Why is that? In Landau theory for magnets, the coefficient of the quadratic term $r|\vec{M}|^2$ disappears at

the critical temperature $r \sim (T - T_c)$. Here, all we have are gradients and nonlinear terms in a Landau theory. In the field theory immediately above, there is no "mass" associated with the tipping vector $\sim \vec{\nabla} f$ of the normal. We could get away from this "self-organized criticality," a consequence of the rotational and translational invariance of the elastic sheet, by changing the boundary conditions of the sheet via introducing an edge tension, similar to a taut drum head. With free boundary conditions, however, we'll get critical phenomena without having to adjust any parameters and and fluctuations will be very important.

5.4.1 Integrating out the in-plane phonons

Since we will focus primarily on the out-of-plane behavior of the sheets (flexural phonons associated with crumpling and wrinkling), we'll trace out the in-plane phonons to obtain a new effective free energy

$$e^{-\tilde{F}/k_B T} \equiv \int \mathcal{D}\underset{\sim}{u}(\underset{\sim}{x}) e^{-F[f, \underset{\sim}{u}]/k_B T}. \tag{5.81}$$

Although somewhat subtle (see below!), this tracing out is possible because the in-plane phonon degrees of freedom only appears quadratically in Eq. 5.79. We'll denote the nonlinear piece of the strain field as A_{ij}

$$A_{ij}(\underset{\sim}{x}) \equiv -\frac{1}{2}(\partial_i f)(\partial_j f), \tag{5.82}$$

where i, j are now being used to index the directions x, y. As mentioned above, this matrix vector potential is the source of geometric frustration in Eq. 5.80, because one cannot in general choose a two component displacement field $\vec{u}(\underset{\sim}{x})$ to cancel out the three components of $A_{ij}(\underset{\sim}{x})$ to produce a vanishing strain energy.

We now decompose the strain field into more general Fourier components,

$$u_{ij}(\underset{\sim}{x}) = u_{ij}^0 + A_{ij}^0 + \sum_{\underset{\sim}{q} \neq 0} \left[\frac{i}{2}(q_i u_j + q_j u_i) - A_{ij}(\underset{\sim}{q}) \right] e^{i\underset{\sim}{q} \cdot \underset{\sim}{x}} \tag{5.83}$$

where the finite q and zero q components of the vector potential are treated separately

$$A_{ij}(\underset{\sim}{q}) = \frac{-1}{2L^2} \int d^2 x e^{-i\underset{\sim}{q} \cdot \underset{\sim}{x}}(\partial_i f)(\partial_j f), \quad A_{ij}^0 = \frac{-1}{2L^2} \int d^2 x (\partial_i f)(\partial_j f). \tag{5.84}$$

To motivate what comes next, recall from studies of, say, electricity and magnetism, that any arbitrary vector field $\vec{V}(\vec{r})$ can be decomposed into a longitudinal part (the gradient of a scalar field), a solenoidal part (the curl of a vector field), up to an additive constant,

$$\vec{V}(\vec{r}) = \vec{\nabla}\phi(\vec{r}) + \vec{\nabla} \times \vec{\Omega}(\vec{r}). \tag{5.85}$$

Our matrix vector potential can be written the same way, by noting that any 2×2 symmetric tensor can be decomposed into a symmetrized longitudinal part

$$A_{ij}(\underset{\sim}{x}) = \underbrace{\frac{1}{2} \left[\partial_i \phi_j(\underset{\sim}{x}) + \partial_j \phi_i(\underset{\sim}{x}) \right]}_{\text{longitudinal}} + \underbrace{P_{ij}^T \Phi(\underset{\sim}{x})}_{\text{transverse}}, \tag{5.86}$$

where the transverse projection operator (to eventually be treated in Fourier space) is

$$P_{ij}^T = \delta_{ij} - \frac{\partial_i \partial_j}{\nabla^2}. \tag{5.87}$$

We can in fact calculate the transverse part of this decomposition by applying P_{ij}^T to project away the longitudinal part of Eq. 5.86

$$P_{ij}^T A_{ij} \equiv \Phi(x) = -\frac{1}{2} P_{ij}^T (\partial_i f)(\partial_j f) \tag{5.88}$$

where the trace of the square of the transverse projection operator and its square are 1, in two dimensions,

$$P_{ij}^T P_{ij}^T = P_{ij}^T P_{ji}^T = P_{ii}^T = 2 - 1 = 1. \tag{5.89}$$

This result also follows from the eigenvalues of the 2×2 projection operator, which are 1 and 0. Recall from Eq. 5.74 that the $\partial_i f$ derivatives describe the tilt of the surface normal undulations, analogous to periodic tiltings that lead to spin waves in the Heisenberg model. We'll soon see that $\Phi(x)$ in Eq. 5.88 leads to quartic interactions between tilts of the surface normals.

On substituting the decomposition Eq. 5.86 into Eq. 5.83, we can express the strain tensor as

$$u_{ij}(x) = w_0^{ij} + \sum_{q \neq 0} \left(\frac{i}{2} \left[q_i w_j(q) + q_j w_i(q) \right] + P_{ij}^T \Phi(q) \right) e^{iq \cdot x}, \tag{5.90}$$

where w_j and w_{ij}^0 are the new shifted variables, and $\Phi(q)$ is the Fourier transform of $\Phi(x)$ (see Eq. 5.93). Here, w_{ij}^0 is the sum of the zero momentum component of the original strain tensor u_{ij} and the nonlinear strain tensor A_{ij}, while w_i is the sum of the displacement fields correspond to the symmetrized derivatives of the in-plane phonon displacement u_i and longitudinal part of the nonlinear strain tensor:

$$w_{ij}^0 = u_{ij}^0 + A_{ij}^0, \quad w_i(q) = u_i(q) + \phi_i(q). \tag{5.91}$$

We don't need the actual functions $\phi_i(x)$ (straightforwardly obtained by applying a longitudinal projection operator to Eq. 5.86), since we'll be integrating out the $w(q)$ modes anyway. Here, the transverse projector in Fourier space is

$$P_{ij}^T(q) = \delta_{ij} - \frac{q_i q_j}{q^2} \tag{5.92}$$

and the Fourier transformed vector potential is

$$\Phi(q) = -\frac{1}{2L^2} \int d^2 x e^{-iq \cdot x} P_{ij}^T (\partial_i f)(\partial_j f), \tag{5.93}$$

where $L^2 = A$ is the area of an $L \times L$ membrane.

It is straightforward now to integrate over the shifted variables, $w_{xx}^0, w_{yy}^0, w_{xy}^0$ and $w(q)$, to get a new effective free energy

$$e^{-\tilde{F}/k_B T} = \int dw_{xx}^0 \int dw_{yy}^0 \int dw_{xy}^0 \int_{q \neq 0} \mathcal{D} w(q) \exp \left[-F(f, w)/k_B T \right]. \tag{5.94}$$

Note first that the elastic (non-bending) part of the free energy in Eq. 5.79 is

$$F_{el} = \int d^2x \left[\mu \left\{ w_{ij}^0 + \sum_{\underset{\sim}{q}\neq 0} \left[\frac{i}{2}(q_i w_j + q_j w_i) + P_{ij}^T \Phi(\underset{\sim}{q}) \right] e^{-i\underset{\sim}{q}\cdot\underset{\sim}{x}} \right\}^2 + \frac{\lambda}{2} \left\{ w_{kk}^0 + \sum_{\underset{\sim}{q}\neq 0} [i\underset{\sim}{q}\cdot\underset{\sim}{w} + \Phi(\underset{\sim}{q})] e^{-i\underset{\sim}{q}\cdot\underset{\sim}{x}} \right\}^2 \right].$$

(5.95)

Since the cross terms linear in w_{ij}^0 in the $\{\cdots\}^2$ pieces vanish because $\int d^2x\, e^{-i\underset{\sim}{q}\cdot\underset{\sim}{x}} = 0$ for $\underset{\sim}{q}\neq 0$, the elastic free energy becomes

$$
\begin{aligned}
F_{el} &= L^2\left[\mu(w_{ij}^0)^2 + \frac{\lambda}{2}(w_{kk}^0)^2\right] + L^2\mu\sum_{\underset{\sim}{q}\neq 0}\left[\frac{1}{4}[q_i w_j(\underset{\sim}{q}) + q_j w_i(\underset{\sim}{q})][q_i w_j(-\underset{\sim}{q}) + q_j w_i(-\underset{\sim}{q})] + |\Phi(\underset{\sim}{q})|^2\right] \\
&\quad + L^2\frac{\lambda}{2}\sum_{\underset{\sim}{q}\neq 0}\left[q_i q_j w_i(-\underset{\sim}{q})w_j(\underset{\sim}{q}) + 2iq_j w_j(\underset{\sim}{q})\Phi(-\underset{\sim}{q}) + |\Phi(\underset{\sim}{q})|^2\right],
\end{aligned}
$$

(5.96)

where we have used $q_i P_{ij}^T(\underset{\sim}{q}) = q_j P_{ij}^T(\underset{\sim}{q}) = 0$. Note that the first term integrates out in Eq. 5.94 to produce an overall constant contribution to $\tilde{F}$. Upon separating out the terms quadratic in $\vec{w}$ and linear in $\vec{w}$, we have

$$
\begin{aligned}
F_{el} &= \frac{L^2}{2}\sum_{\underset{\sim}{q}\neq 0}(2\mu + \lambda)|\Phi(\underset{\sim}{q})|^2 + \frac{L^2}{2}\sum_{\underset{\sim}{q}\neq 0}\left[\mu q^2\left(\delta_{ij} - \frac{q_i q_j}{q^2}\right) + (2\mu + \lambda)q^2\frac{q_i q_j}{q^2}\right]w_j(\underset{\sim}{q})w_i(-\underset{\sim}{q}) \\
&\quad + L^2 i\lambda\sum_{\underset{\sim}{q}\neq 0}q_j w_j(\underset{\sim}{q})\Phi(-\underset{\sim}{q}) + \text{const.}
\end{aligned}
$$

(5.97)

For each $\underset{\sim}{q}\neq 0$, we need to do a two-dimensional integral of the form

$$\int dw_1(\underset{\sim}{q})\int dw_2(\underset{\sim}{q})e^{-D_{ij}w_i w_j/4 + B_j w_j} = \text{const} \times \exp\left[-B_i D_{ij}^{-1}B_j/4\right], \qquad (5.98)$$

where

$$
\begin{aligned}
D_{ij}(\underset{\sim}{q}) &= \frac{L^2}{2k_B T}\left[\mu q^2\left(\delta_{ij} - \frac{q_i q_j}{q^2}\right) + (2\mu + \lambda)q^2\frac{q_i q_j}{q^2}\right] \quad &(5.99) \\
D_{ij}^{-1}(\underset{\sim}{q}) &= \frac{2k_B T}{L^2\mu q^2}\left(\delta_{ij} - \frac{q_i q_j}{q^2}\right) + \frac{2k_B T}{L^2(2\mu + \lambda)q^2}\frac{q_i q_j}{q^2} \quad &(5.100) \\
B_j(\underset{\sim}{q}) &= \frac{L^2\lambda i}{k_B T}q_j\Phi(-\underset{\sim}{q}). \quad &(5.101)
\end{aligned}
$$

On carrying out the functional integrals in Eq. 5.94, we find (including the first term of Eq. 5.97),

$$
\begin{aligned}
\tilde{F} &= \text{const.} + \frac{1}{2}\kappa\int d^2x(\nabla^2 f)^2 + \frac{L^2}{2}\sum_{\underset{\sim}{q}\neq 0}(2\mu + \lambda)|\Phi(\underset{\sim}{q})|^2 \\
&\quad - \frac{L^2}{4}\sum_{\underset{\sim}{q}\neq 0}\lambda^2 q_i q_j|\Phi(\underset{\sim}{q})|^2\left[\frac{2}{\mu q^2}\left(\delta_{ij} - \frac{q_i q_j}{q^2}\right) + \frac{2}{(2\mu + \lambda)q^2}\frac{q_i q_j}{q^2}\right] \\
&= \text{const.} + \frac{1}{2}\kappa\int d^2x(\nabla^2 f)^2 + \frac{L^2}{2}\sum_{\underset{\sim}{q}\neq 0}|\Phi(\underset{\sim}{q})|^2\left[(2\mu + \lambda) - \frac{\lambda^2}{2\mu + \lambda}\right]
\end{aligned}
$$

(5.102)

$$
= \text{const.} + \frac{1}{2}\kappa\int d^2x(\nabla^2 f)^2 + \frac{L^2 Y}{2}\sum_{\underset{\sim}{q}\neq 0}|\Phi(\underset{\sim}{q})|^2, \qquad (5.103)
$$
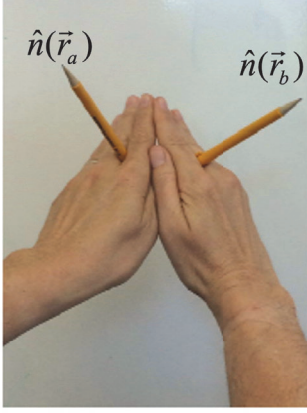
A longitudinal spin wave fluctuation only requires low energy bending
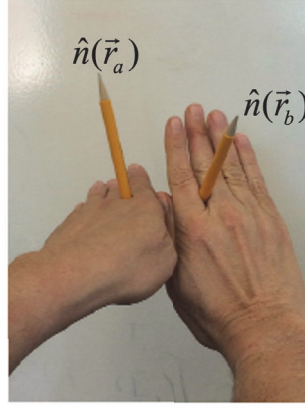
A transverse spin wave fluctuation requires energetically costly stretching, unless this happens along a cut

Figure 5.6: Excitations where the surface normal varies longitudinally along the direction of change (left) cost much less energy than excitations where the variation in the surface normal is transverse to the direction of change, which would require stretching or tearing the surface (right).

where $Y = 4\mu(\mu+\lambda)/(2\mu+\lambda)$ is the Young's modulus. On returning to real space,

$$\Phi(q) = \frac{1}{L^2}\int d^2x \Phi(x)e^{-iq\cdot x}, \quad \Phi(x) = -\frac{1}{2}P_{ij}^T(q)(\partial_i f)(\partial_j f). \tag{5.104}$$

we have

$$\tilde{F} = \text{const.} + \frac{1}{2}\kappa\int d^2x(\nabla^2 f)^2 + \frac{YL^2}{2}\int\frac{d^2x}{L^2}\int\frac{d^2x'}{L^2}\Phi(x)\Phi(x')\underbrace{\sum_{q\neq 0}e^{iq\cdot(x'-x)}}_{L^2\delta(x-x')} \tag{5.105}$$

Thus, the overall effective energy simplifies to,

$$\tilde{F}(f) = \text{const.} + \frac{1}{2}\kappa\int d^2x(\nabla^2 f)^2 + \frac{Y}{8}\int d^2x\left[P_{ij}^T(\partial_i f)(\partial_j f)\right]^2. \tag{5.106}$$

We've now reduced a three-coupling-constant free energy to a two-coupling-constant field theory, with the Young's modulus $Y = 4\mu(\mu+\lambda)/(2\mu+\lambda)$ that controls the nonlinear interactions and the bending rigidity κ.

Notice the couplings between flexural phonons embodied in the second term. We're now ready to answer the question: What happens when we take the liquid membrane Gaussian field theory in Sec. 5.3 and add nonzero $Y \neq 0$ to impose the constraint of a nonzero shear modulus? On returning to Fourier space,

$$f(x) = \sum_q e^{iq\cdot x}f(q), \tag{5.107}$$
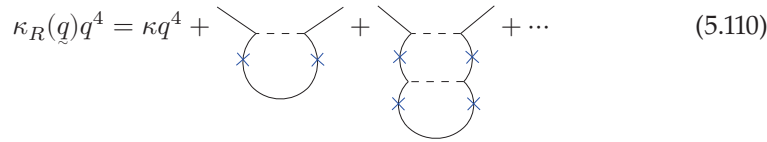
the effective free energy becomes

$$\tilde{F}[f(q)] = \frac{1}{2}\kappa L^2\sum_q |q|^4|f(q)|^2 \tag{5.108}$$

$$+ \frac{YL^2}{8}\sum_{\substack{q_1+q_2=q\neq 0 \\ q_3+q_4=-q\neq 0}}\left[q_{1i}P_{ij}^T(q)q_{2j}\right]\left[q_{3i}P_{ij}^T(q)q_{4j}\right]f(q_1)f(q_2)f(q_3)f(q_4).$$

What is the physical meaning of the second, nonlinear, term in the free energy? As mentioned earlier in this chapter, we can think of the derivatives of f with respect to x_1 and x_2 as vectors associated with the normals tipping away from the $\hat{z}$-direction. This second term gives a strong penalty for certain types of tipping. For example, if the tipping varies longitudinally along the direction of change (like longitudinal spin waves), then the non-linear interactions are not activated at all due to the transverse projection operator. On the other, if the change in tipping is transverse to the direction of change, that will incur a severe penalty associated with the Young's modulus $Y = 4\mu(\mu + \lambda)/(2\mu + \lambda)$ in the second term (see Figure 5.6). In fact, the only way this type of transverse spin wave can happen is if the surface stretches or tears. The nonlinear terms give us the interactions between spin-waves, with a quartic vertex represented by the following,

$$\tag{5.109}$$

where the slashes represent derivatives and each pair of connected solid lines carries a transverse projection operator. We can now do perturbation theory in Y (no renormalization group yet, but that's coming later). Graphically, the bending rigidity κ is renormalized as

$$\kappa_R(\underset{\sim}{q})q^4 = \kappa q^4 + \qquad + \qquad + \cdots \tag{5.110}$$

Note that the following Feynman graph vanishes,

$$, \tag{5.111}$$

because the internal loop includes a transverse projection operator, which has to be evaluated for $q_1 + q_2 = \underset{\sim}{q} \neq 0$. However, momentum conservation at the vertex of the graph requires $q = 0$.

Let's evaluate the lowest order correction to the bending rigidity in Eq. 5.110 in more detail:

$$\kappa_R(\underset{\sim}{q}) = \kappa + \frac{k_B T Y}{4} \int \frac{d^2 k}{(2\pi)^2} \frac{\left[\hat{q}_i P_{ij}^T(\underset{\sim}{k})\hat{q}_j\right]^2}{\kappa|q + \underset{\sim}{k}|^4}. \tag{5.112}$$

Note that the first order correction is positive, so thermal fluctuations *stiffen* the sheet polymer. In fact, this correction diverges in an infinite system due to the momentum factors in the denominator. Let's study this diverging correlation length in more detail. On taking the limit of the external momentum vanishing $q \to 0$ and noting that $\left[\hat{q}_i P_{ij}^T(k)\hat{q}_j\right]^2 = \sin^2\theta$ where θ is the angle between $\underset{\sim}{k}$ and $\underset{\sim}{q}$, Eq. 5.112 becomes, after carrying out an angular average,

$$\lim_{\underset{\sim}{q}\to 0} \kappa_R(\underset{\sim}{q}) \approx \kappa + \frac{k_B T Y}{16\pi\kappa} \int_{\pi/L}^{\pi/a} \frac{k dk}{k^4} = \kappa\left[1 + \frac{k_B T}{\kappa}\frac{1}{32\pi^3}\frac{Y L^2}{\kappa} + \cdots\right], \tag{5.113}$$

where L, the linear size of the sheet polymer, provides an infrared cut off and a is a microscopic monomer spacing. On a positive note, for this perturbative calculation,

we expect $\frac{k_B T}{\kappa} \ll 1$ (for e.g. graphene $\frac{k_B T}{\kappa} \approx \frac{1}{50} \ll 1$ at room temperature). In addition, the numerical, factor $\frac{1}{32\pi^3} \ll 1$. However, the third factor (the dimensionless Foppl-von-Karmen number characterizing a thin elastic sheet), using $L = 10\mu$m and elasticity parameters extracted from graphene experiments, turns out to be huge

$$\frac{YL^2}{\kappa} = 10^{11},\tag{5.114}$$

and completely overwhelms the smallness of the other two factors. So simple perturbation theory explodes in the large L (i.e. large sample size) limit. By looking at when the correction becomes comparable to unity, one can get a Ginzburg-like criterion for the size of the system beyond which thermal fluctuations start to matter. For example, how big can our piece of graphene be before these thermal fluctuations at room temperature take over? The answer (as discussed in more detail below) turns out to be only 3 Angstroms!

There are two things we can do in the face of this problem. One is a self-consistent graphical resummation. Although this approach is useful, we know from the earlier parts of this book that the ultimate solution will be to use the renormalization group methods!

5.4.2 Self-consistent theory

As we saw in Eq. 5.110, there's a whole tower of strongly diverging Feynman graphs at each order of perturbation theory. It turns out that summing up the most divergent of these higher-order graphs is equivalent to doing propagator renormalization in the denominator of this integral [92]. We can solve for $\kappa_R(q)$ self consistently by replacing κ with $\kappa_R(q + \underset{\sim}{k})$ in the denominator of the integral in Eq. 5.112,

$$\kappa_R(\underset{\sim}{q}) = \kappa + \frac{k_B T Y}{4} \int \frac{d^2 k}{(2\pi)^2} \frac{\left[\hat{q}_i P_{ij}^T(k)\hat{q}_j\right]^2}{\kappa_R(\underset{\sim}{q} + \underset{\sim}{k})|\underset{\sim}{q} + \underset{\sim}{k}|^4}\tag{5.115}$$

We're going to take a different limit. Instead of directly letting $q \to 0$ right away, we'll first take $L \to \infty$ limit while fixing q, and take $q \to 0$ later. The fixed external $\underset{\sim}{q}$ provides an alternative way to cut off infrared divergence in the integral in Eq. 5.115 and prevent it from diverging,

$$\kappa_R(\underset{\sim}{q}) = \kappa + \text{const.}\frac{k_B T Y}{\kappa_R(q)q^4} \int_0^q k\,dk = \kappa + \text{const} \times \frac{k_B T Y}{\kappa_R(\underset{\sim}{q})q^2}.\tag{5.116}$$

Note that the correction is still positive (the membrane is stiffening under thermal fluctuations) but no longer diverging provided $q > 0$. When $q \neq 0$, we can solve the algebraic equation for $\kappa_R(q)$. If we focus on the long wavelengths limit $\underset{\sim}{q} \to 0$, the second term dominates and the first term drops out, leading to [89],

$$\kappa_R(q) \sim \frac{\sqrt{k_B T Y}}{q}.\tag{5.117}$$

Thus, the bending rigidity is scale dependent and diverges at long wavelengths. This is a breakdown of Hooke's law, where elastic constants at long wavelengths are expected to be truly constant. Here, instead, the bending rigidity is a strong function of the system size $L \sim \pi/q$! Note that the nonzero elasticity constants, in
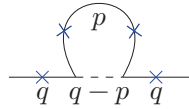
particular the Young's modulus Y, as well as thermal fluctuations and associated entropic effects, play a key role here. We would not find the same stiffening effect with increasing system sizes for e.g. a liquid membrane, where $Y = \mu = 0$: Indeed, the renormalized bending rigidity of liquid membrane *softens* logarithmically for large system sizes [93].
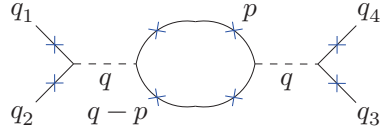
5.5 Renormalization group treatment

In general, it is often conveninent to study D-dimensional elastic manifolds embedded in $d = D + 1$ dimensions and do iterative renormalizations using perturbation theory in $\epsilon = 4 - D$ [94]. However, we can also work with Eq. 5.108 directly in $d = 3$ and $D = 2$ using an approximate momentum shell renormalization group [95]. In line with the renormalization group procedure developed in this book, we'll have a flexural phonon rescaling factor b^{ζ_f} and a spatial rescaling factor b, with

$$f(\underset{\sim}{x}) = b^{\zeta_f} f'(\underset{\sim}{x}'), \quad \underset{\sim}{x}' = \underset{\sim}{x}/b. \tag{5.118}$$

To one loop order, the coupling constants get modified by the diagrams such as the following:

 renormalizes κ (5.119)

 renormalizes Y (5.120)

For notational convenience, we will absorb the temperature into the elasticity couplings and set $\bar{\kappa} \equiv \kappa/k_B T$, $\bar{Y} \equiv Y/k_B T$. The renormalization recursion relations that follow from the momentum shell version of the diagrams in Eq. 5.119 and 5.120 are then

$$\frac{d\bar{\kappa}(\ell)}{d\ell} = (2\zeta_f - 2)\bar{\kappa}(\ell) + \frac{3\bar{Y}(\ell)}{16\pi\bar{\kappa}\Lambda^2} \tag{5.121}$$

$$\frac{d\bar{Y}(\ell)}{d\ell} = (4\zeta_f - 2)\bar{Y}(\ell) - \frac{3\bar{Y}^2(\ell)}{32\pi\bar{\kappa}^2(\ell)\Lambda^2}, \tag{5.122}$$

so the bending rigidity is enhanced by the nonlinearities while the Young's modulus softens. We now choose ζ_f, the flexural phonon rescaling factor, to keep $\kappa(\ell)$ fixed, which leads to

$$\zeta_f = 1 - \frac{3\bar{Y}}{32\pi\bar{\kappa}^2\Lambda^2}. \tag{5.123}$$

This choice transforms the recursion relation for $\bar{Y}(\ell)$ into [95],

$$\frac{d\bar{Y}(\ell)}{d\ell} = 2\bar{Y} - \frac{15\bar{Y}^2}{32\pi\bar{\kappa}^2\Lambda^2}. \tag{5.124}$$

Thus, as shown in Figure 5.7, within this perturbative renormalization group theory, the physics of a $D = 2$ elastic sheet fluctuating in $d = 3$ dimensions always flows to a nontrivial fixed point with $\bar{Y} = \bar{Y}^* = \frac{64\pi}{15}\kappa^2\Lambda^2$, whether the bare value of $\bar{Y}$ "starts out" big or small. The flexural phonon rescaling factor at this attractive fixed point is given by

$$\zeta_f^* = 1 - \frac{3\bar{Y}^*}{32\pi\kappa^2\Lambda^2} = 1 - \frac{2}{5} \equiv 1 - \frac{\eta}{2}, \quad \eta = \frac{4}{5}. \tag{5.125}$$

It is interesting to note that this *new* sheet polymer critical exponent η (the self-consistent theory of Ref. [92] gives $\eta = 1$) also describes how flexural phonons couple to the *quantum* Dirac electrons in the fluctuating graphene sheet [96, 97].

Why does the momentum shell renormalization group work here? If we look at the recursion relation in Eq. 5.124 for the Young's modulus in terms of the bare coupling constants κ and Y, we have

$$\frac{dY}{d\ell} = 2Y\left[1 - \frac{15}{64\pi}\frac{k_B T Y a^2}{\kappa}\frac{a^2}{\kappa}\right], \tag{5.126}$$

where we have set $a \approx \Lambda^{-1}$. Because $k_B T/\kappa \lesssim O(1)$ and $Ya^2/kappa = O(1)$ for graphene, the correction is small.

We can now study how the renormalized bending rigidity,

$$\kappa_R^{-1}(\underset{\sim}{q}) = L^2 q^4 \langle|f(\underset{\sim}{q})|^2\rangle, \tag{5.127}$$

changes under the renormalization group. If we calculate the RHS of this equation using the Gaussian ensemble without interactions, we have $\langle|f(\underset{\sim}{q})|^2\rangle_0 = \frac{1}{L^2\kappa q^4}$ from the equipartition theorem, and the renormalized bending rigidity would be equal to the bare bending rigidity $\kappa_R = \kappa$. For the more general case including in-plane elasticity, we can use the renormalization group to map this hard problem (diverging Feynman graphs for small q) onto an easy problem, at large values of q,

$$\kappa_R(\underset{\sim}{q}) = b^{2-2\zeta_f}\kappa_R(b\underset{\sim}{q}). \tag{5.128}$$

Because $q \rightarrow bq$, as usual for momentum shell renormalization groups, small wavevectors are mapped to large wave vectors where the integrals describing nonlinear corrections don't diverge as badly. The exponent in the prefactor, if we go to long enough wavelengths, is determined by the value at the fixed point (Eq. 5.125)

$$\zeta_f^* = 1 - \frac{\eta}{2}. \tag{5.129}$$

Putting everything together, we arrive at

$$\kappa_R(\underset{\sim}{q}) = b^\eta \kappa_R(b\underset{\sim}{q}) \sim \frac{1}{|\underset{\sim}{q}|^\eta}, \quad \eta = \frac{4}{5}, \tag{5.130}$$

where $\underset{\sim}{q}$ is providing a cutoff to the infrared divergence. We see that the bending rigidity is again strongly wave vector dependent. Since the wave vector at long wavelengths for an $L \times L$ sheet is $q = |\underset{\sim}{q}| \sim \frac{1}{L}$, we have, again, a scale-dependent renormalized elastic constant:
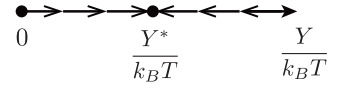
$$\kappa_R \sim L^\eta. \tag{5.131}$$

Figure 5.7: Renormalization group flow diagram of the Young's modulus of a thermally fluctuating sheet.

Note that here, unlike that of typical problems in conventional critical phenomena, η is not tiny but has a value of 0.8 (a more accurate approximation is $\eta \approx 0.85$ [98]). It turns out, as we'll show shortly, that this η is easily large enough to give us long range order in the normals of a two-dimensional elastic sheet, thus escaping the Hohenberg-Mermin-Wagner theorem.

To see that the diverging $\kappa_R(q)$ implies long range order in the normals of the sheet, let's again assume symmetry breaking and long range order in the normals and see if the fluctuations about this state are small. If the fluctuations diverge, then the assumption of long range order is untrue. If the fluctuations remain finite, then we indeed have long range order. As in our discussion of liquid membranes, the normals are given by

$$\hat{n}(x_1, x_2) \approx \frac{1}{\sqrt{1 + |\nabla f|^2}} \begin{pmatrix} -\partial_1 f \\ -\partial_2 f \\ 1 \end{pmatrix} \tag{5.132}$$

and the projection of the normals along the "preferred" z-axis direction is

$$\langle \hat{n} \cdot \vec{e}_3 \rangle = \langle \cos \theta \rangle = \left\langle \frac{1}{\sqrt{1 + |\nabla f|^2}} \right\rangle. \tag{5.133}$$

Upon expanding both the cosine and square root in the above expression, we now find the fluctuations in the tipping angle to be

$$\langle \theta^2(x) \rangle = \langle |\nabla f|^2 \rangle = \int \frac{d^2 q}{(2\pi)^2} \frac{q^2 k_B T}{\kappa_R(q) q^4}. \tag{5.134}$$

This integral would diverge if κ_R was replaced by the bare bending rigidity κ (as we did for liquid membranes). However, with the renormalized bending rigidity $\kappa_R(q) \sim q^{-\eta}$, we have

$$\langle \theta^2(x) \rangle \sim \frac{k_B T}{\kappa} \int_0^\Lambda \frac{q dq}{q^{2-\eta}} < \infty, \quad \text{if } \eta > 0, \tag{5.135}$$

and the angle fluctuations are prevented from diverging since $\eta = 4/5 > 0$. Thus, we have long range order in the normals of fluctuating elastic sheet polymers in $d = 2$.

In summary, although tethered surfaces (another name for elastic sheet polymers) are asymptotically flat at low temperatures, the thermally-induced wrinkles stiffen the bending rigidity in a scale-dependent way. The study of "tethered surfaces" found initial motivation in biological systems, such as the fishnet-like spectrin skeleton of red blood cells [85]. However, starting in the 1980's, there have been searches for covalent analogs of flexible sheet polymers. Examples include graphite oxide membranes[13], the rag phase of MoS2[12], and most recently, free-standing graphene[14]. In the following sections, we provide an overview of recent developments in the study of tethered surfaces. We'll see that both surface topology and a fluctuating metric tensor will play very important roles in the physics.

5.6 Overview of the statistical mechanics of atomically thin plates

In problems of elastic sheets where both bending and stretching energies play an important role, one dimensionless number is of particular importance: the Foppl-von Karman number vK. Given that there are now evidence for a flat phase of graphene [14], one challenge is to see if we can access a crumpled phase as well. If the latter case occurs for materials like graphene, what will happen to the Dirac graphene electrons that would inhabit this crumpled landscape? One way we may be able to access the crumpled phase through perforations. If the graphene becomes lacy or tenuous enough, it might be able to undergo a crumpling transition [84].

5.6.1 Nonlinear Foppl-von Karman equations at $T = 0$

The zero temperature theory sketched above, which we have promoted to the finite temperature statistical mechanics of elastic membranes, goes back to Foeppl and von Karman in 1904. We have already encountered this energy in our studies of the elastic sheet,

$$F(f, \underset{\sim}{u}) = \frac{1}{2} \int d^2 x \big[\underbrace{\kappa \left(\nabla^2 f(\underset{\sim}{x}) \right)^2}_{\text{bending energy}} + \underbrace{2 \mu u_{ij}^2(\underset{\sim}{x}) + \lambda u_{kk}^2(\underset{\sim}{x})}_{\text{stretching energy}} \big]. \tag{5.136}$$

As we have seen, these out-of-plane (flexural) phonons that appear in the strain tensor in Eq. 5.80 can escape softly into the third dimension, where the "soft" terminology emphasizes that the bending term is quartic in the wave vector when passing to Fourier space. As we have found at finite temperatures, this soft escaping plays an important role in the statistical mechanics, giving rise to a nonlinear critical field theory without needing to tune to the temperature to some special value.

To put the results for thermalized membranes into context, we now discuss the nonlinear Foppl-von-Karman equations obtained by taking functional derivatives of Eq. 5.136, and minimizing Eq. 5.136 at $T = 0$. Given a set of forces applied to an elastic sheet described by a stress tensor σ_{ij} and a strain tensor u_{ij}, we expect they are connected via a (nonlinear) Hooke's law, as in the first part of Eq. 5.138 below. On requiring the forces to balance at every point at a static functional minimum, the nonlinear stress tensor σ_{ij} have to satisfy the zero divergence condition due to force balance

$$\partial_i \sigma_{ij} = 0. \tag{5.137}$$

In electrostatics, when we require $\vec{\nabla} \cdot \vec{B} = 0$, we can write the magnetic field $\vec{B}$ as a the curl of some vector potential $\vec{B} = \vec{\nabla} \times \vec{A}$. The analogous simplification here is to write the strain σ_{ij} via the following ansatz

$$\sigma_{ij}(\underset{\sim}{x}) = 2 \mu u_{ij}(\underset{\sim}{x}) + \lambda \delta_{ij} u_{kk}(\underset{\sim}{x}) \equiv \epsilon_{im} \epsilon_{jn} \partial_m \partial_n \chi(\underset{\sim}{x}), \tag{5.138}$$

which automatically satisfies Eq. 5.137 and where $\chi(\underset{\sim}{x})$ is known as the Airy stress function, analogous to the scalar potential in electrostatics [88]. We can take this ansatz and substitute it back into the energy, and do a functional minimization of the

free energy over $f(\underset{\sim}{x})$ and $\chi(\underset{\sim}{x})$ to get the ground state at zero temperature, subject to various boundary conditions, as discussed in Ref. [88].

On minimizing the energy in Eq. 5.136 over $f(\underset{\sim}{x})$ and $\chi(\underset{\sim}{x})$, we get the Foppl-von Karman equations

$$\kappa \nabla^4 f = \frac{\partial^2 \chi}{\partial y^2}\frac{\partial^2 f}{\partial x^2} + \frac{\partial^2 \chi}{\partial x^2}\frac{\partial^2 f}{\partial y^2} - 2\frac{\partial^2 \chi}{\partial x \partial y}\frac{\partial^2 f}{\partial x \partial y} \tag{5.139}$$

$$\frac{1}{Y}\nabla^4 \chi = -\frac{\partial^2 f}{\partial x^2}\frac{\partial^2 f}{\partial y^2} + \left(\frac{\partial^2 f}{\partial x \partial y}\right)^2 = \text{Gaussian curvature} .$$

The Lamé elastic coefficients again get bundled together in the Young's modulus Y,

$$Y = \frac{4\mu(\mu + \lambda)}{2\mu + \lambda}, \tag{5.140}$$

whose reciprocal enters in front of the Laplacian squared acting on χ in the second equation. These equations are highly nonlinear; the first equation is bilinear in χ and f on the right hand side. The quadratic terms in f in the second equation act as a source term for χ, a biharmonic analog of the electrostatic potential. These equations can be thought of as a two-dimensional relative of general relativity (in fact, they preceded the theory of general relativity by about a decade), and complicated via the first equation by their dependence on the extrinsic curvature in addition to the intrinsic Gaussian curvature. The later acts as a source term for the Airy stress function in the second line of Eq. 5.139. Note also that κ, which is typically quite small for sheet polymers like graphene, multiplies the highest derivative in the first line. Similarly, the stiff Young's modulus Y of materials like graphene means another small parameter, $1/Y$, multiplies the highest derivative in the second equation. Such combinations are often a sign of singular behavior in nonlinear partial differential equations. Exact solutions to Eqs. 5.139 were only available in special cases.

The parameter that controls the physics at zero temperature is the Foppl-von-Karman number vK$\equiv \gamma = YL^2/\kappa \gg 1$(analogous to a Reynolds number in fluid mechanics), where L is the linear system size. This number *has* to come in when we non-dimensionalize the equations. For a sheet of size L, upon scaling the vertical displacement $f = L\tilde{f}$ and $\chi = YL^2\tilde{\chi}$, the Foppl-von-Karman equations in Eq. 5.139 can be written more compactly as,

$$\frac{1}{\gamma}\nabla^4 \tilde{f} = \frac{\partial^2 \tilde{\chi}}{\partial y^2}\frac{\partial^2 \tilde{f}}{\partial x^2} + \frac{\partial^2 \tilde{\chi}}{\partial x^2}\frac{\partial^2 \tilde{f}}{\partial y^2} - 2\frac{\partial^2 \tilde{\chi}}{\partial x \partial y}\frac{\partial^2 \tilde{f}}{\partial x \partial y} \tag{5.141}$$

$$\nabla^4 \tilde{\chi} = -\frac{\partial^2 \tilde{f}}{\partial x^2}\frac{\partial^2 \tilde{f}}{\partial y^2} + \left(\frac{\partial^2 \tilde{f}}{\partial x \partial y}\right)^2, \quad \gamma = YL^2/\kappa \tag{5.142}$$

where the dimensionless Foppl-von-Karman number γ is the only parameter present; its inverse multiplies the biharmonic operator ∇^4 in the first equation. Note that in most 2d systems, γ is huge. For example, a crumpled aluminum foil or paper of size L, thickness h, and two-dimensional Poisson ratio $\nu = \lambda/(2\mu + \lambda)$ has the following parameters: $L \approx 8.5$in, $h \approx 0.1$mm, $\nu \approx 0.25$. The Foppl-von-Karman number γ

follows from [88],

$$\kappa = E_3 h^3 / \left[12 \left(1 - \nu^2 \right) \right] \tag{5.143}$$

$$Y = E_3 h \tag{5.144}$$

$$E_3 = \text{3d isotropic Young's modulus} \tag{5.145}$$

$$\gamma = Y L^2 / \kappa = 12 (L/h)^2 \left(1 - \nu^2 \right) \approx 4 \times 10^7 \tag{5.146}$$

Note that vK$= \gamma$ scales as $(L/h)^2$!

For a $L = 10\mu$ square of graphene, γ is even larger. Upon inserting the estimates from Ref. [14],

$$Y = 20 eV/A^2 \tag{5.147}$$

$$\kappa = 1.2 eV \tag{5.148}$$

we obtain

$$\gamma = Y L^2 / \kappa \approx 10^{12}, \tag{5.149}$$

where the $T = 0$ estimates of Y and κ can be obtained using quantum mechanical density functional theory (DFT). Note than when the sheet is wrinkled due to thermal fluctuations or crumpling, $\nabla^4 f$ shoots up, but is multiplied only by a very small $1/\gamma$ prefactor in Eq. 5.141. This combination leads to rich physics even when $T = 0$, much like the Navier-Stokes equations at high Reynolds numbers.

5.6.2 Thin solid shells and structures

The FvK equations at zero temperature have many interesting applications, such as in the physics of thin solid sheets and shells [88]. They control the growth and shape of plant leaves and flower petals, the strength of egg shells, and the stability of cylindrical shells used in space rockets. NASA scientists had to solve the FvK equations to find the vertical acceleration threshold at which a rocket fuselage would collapse. The FvK equations also find many applications in nanoscience. We've already mentioned graphene and the cytoskeleton of red blood cells. Other examples include bacterial cell walls and viral capsids, which must resist osmotic pressure. These objects are small enough that Brownian motion due to thermal agitation is important, as we explore in more detail below.

Recall that the phonon fields in the original free energy are only quadratic in u_i. We could thus integrate them out, leaving only the out-of-plane f field. As discussed above, we can then do perturbation theory at low temperatures $k_b T / \kappa \ll 1$ and find the first order correction in the infrared limit to be dependent on the system size through the vK number $\gamma = Y L^2 / \kappa$,

$$\lim_{|\underset{\sim}{q}| \to 0} \kappa_R (\underset{\sim}{q}) \approx \kappa \left[1 + 3\gamma k_B T / \left(32 \pi^3 \kappa \right) + ... \right]. \tag{5.150}$$

However, since the FvK number is huge even for relatively small $\sim 10\mu$-sized sheets and diverges with system size, first order perturbation theory is not enough. As we have seen, we could try to sum up all diverging higher order graphs (essentially calculating the self energy via propagator renormalization). If we assume that the Young's modulus Y is a scale-independent constant, we can solve for $\kappa_R(\underset{\sim}{q})$ self

consistently to obtain $\kappa_R(q) \sim 1/q$ [92]. Thus, the system becomes stiffer and stiffer as we go to longer wavelengths, allowing for long range order and the existence of a flat phase, even in the presence of thermal fluctuations. Alternatively, we could carry out the simplified renormalization group calculation for a membrane directly in $D = 2$, as we have seen in Eq. 5.130, which gives $\kappa_R(q) \sim 1/q^\eta$ with $\eta = 4/5$.

By a slight extension of the calculations in the previous section, given that $\kappa_R(q) \approx \kappa/(\ell_{\rm th}q)^\eta$ it can be shown that the normal-normal correlation function at finite temperature decays to a nonzero constant as a power law [95],

$$\lim_{[x_a - x_b] \to \infty} \langle \hat{n}\left(x_a\right) \cdot \hat{n}\left(x_b\right)\rangle \approx 1 - \frac{k_B T}{2\pi\kappa} \left[\eta^{-1} + \ln\left(l_{th}/a_0\right)\right] + C\frac{k_B T}{\kappa}\left(\frac{l_{th}}{|x_a - x_b|}\right)^\eta \tag{5.151}$$

Note that the decay to a constant for large $|\vec{r}_a - \vec{r}_b|$ is controlled by the exponent η. Recall that $\eta = 1$ in the self consistent approximation, but $\eta \approx 4/5$ using our renormalization group calculations directly for a $D = 2$ elastic manifold embedded in $d = 3$. As we have discussed, the thermal length scale $\ell_{\rm th}$ can be estimated from when $\gamma \equiv Y\ell_{\rm th}^2/\kappa$ in Eq. 5.150 is big enough so that the correction to κ_R is comparable to its bare value,

$$\ell_{\rm th} \approx {\rm const.}\sqrt{\frac{\kappa^2}{k_B T Y}}. \tag{5.152}$$

5.6.3 A more sophisticated renormalization group for thermalized membranes

One can also work out a more complete and accurate renormalization group theory for elastic sheets without integrating out the in-plane-phonons for general D-dimensional elastic manifolds embedded in d dimensions with energy.

$$E = \frac{1}{2}\int d^2x \left[\kappa\left(\nabla^2 f(x)\right)^2 + 2\mu u_{ij}^2(x) + \lambda u_{kk}^2(x)\right] \tag{5.153}$$

$$u_{ij}(x) = \frac{1}{2}\left[\frac{\partial u_i(x)}{\partial x_j} + \frac{\partial u_j(x)}{\partial x_i} + \frac{\partial f(x)}{\partial x_i}\frac{\partial f(x)}{\partial x_j}\right] \tag{5.154}$$

with the full partition function [94]

$$\mathcal{Z} = \int \mathscr{D}\bar{u}\left(x_1, x_2\right)\int \mathscr{D}f\left(x_1, x_2\right)\exp\left(-E/k_B T\right) \tag{5.155}$$

Aronovitz and Lubensky defined rescaled running dimensionless coupling constants, similar in spirit to those in the calculations we've been doing [94],

$$\bar{\mu}(\ell) = k_B T \mu a_0^2/\kappa^2; \quad \bar{\lambda}(\ell) = k_B T \lambda a_0^2/\kappa^2 \tag{5.156}$$

and the scale dependent Young's modulus

$$Y(\ell) = \frac{4\mu(\ell)[\mu(\ell) + \lambda(\ell)]}{2\mu(\ell) + \lambda(\ell)}. \tag{5.157}$$

The renormalization group flows in Figure 5.8 show a Foeppl-von Karman (FvK) fixed point at zero temperature. However, at any finite temperature, the system crossees over to a stable thermal FvK fixed point, with a set of critical exponents
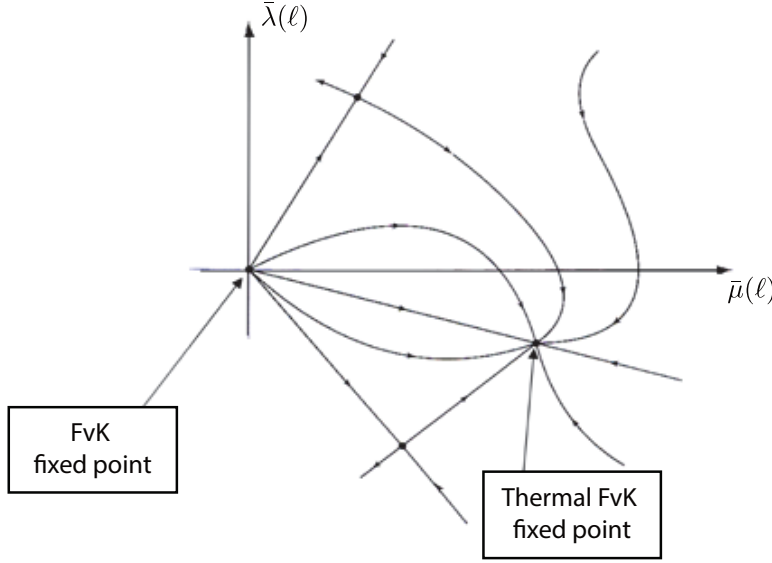
FvK
fixed point

Thermal FvK
fixed point

Figure 5.8: Renormalization group flows for thermally excited thin plates. $\bar{\lambda}(\ell)$ and $\bar{\mu}(\ell)$ are the renormalized 2D Lamé coefficients defined in Eq. 5.156.

given below. As discussed above, it will be important to look at these RG flows for elastic sheets with dimensions $L \gtrsim \ell_{\mathrm{th}}$. Aronovitz and Lubensky originally did their calculations with manifold dimension $D = 4 - \epsilon$ and fixed embedding dimension d, and set $\epsilon = 2$ and $d = 3$. The other two hyperbolic fixed points are probably tricritical points, beyond which there likely exist first order phase transitions. Note that the stable fixed point leads to a renormalized Poisson ratio $\nu_R = \lambda_R/(2\mu_R + \lambda_R)$, which is negative. Thus, at this fixed point, ν_R is not arbitary but assumes the universal value of $\nu_R = -1/3$ to lowest order in ϵ. Note that this universal value is negative! As mentioned above, this strange behavior is qualitatively consistent with the response of wrinkled paper: when we pull out the wrinkled piece of paper in one direction, it also expands in the other direction. The wrinkles can be thought of as a proxy for thermal fluctuations.

The most accurate calculations for thermally excited elastic membranes are probably those made using the self-consistent screening approximation. [98, 99]. The results can be summarized in terms of running scale-dependent coupling constants with two critical exponents,

$$\kappa_R(\ell) \approx \kappa \left(\ell/l_{th}\right)^{\eta} \tag{5.158}$$
$$Y_R(\ell) \approx Y(l_{th}/\ell)^{\eta_u} \tag{5.159}$$
$$\eta \approx 0.82, \quad \eta_u \approx 0.36 \tag{5.160}$$

It can be shown that these two exponents are related by rotational invariance of the elastic manifold, $2\eta + \eta_u = 2$ [94]. Note that the bending rigidity gets stiffer at long length scales, while the Young's modulus gets softer at long length scales. Thus, the elastic "constants" κ and Y are not constants, but depend instead on the length scale of the measurement. (Analogous things happen in metallic wires and sheets with quenched random disorder, where a simple, scale-independent Ohm's law parametrized by a resistivity no longer describes the physics at long wavelengths [100].)
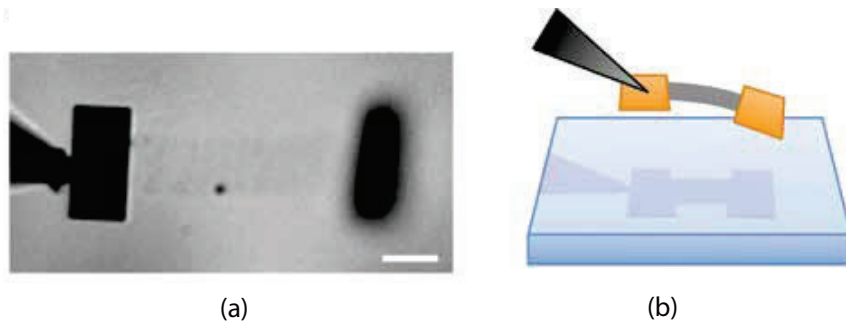
(b)

Figure 5.9: Experimental setup for measuring the spring constant of graphene. Scale bar in (a) indicates 10μm. Figure adapted from Ref. [14].

5.6.4 Experiments on graphene cantilevers

Some of the ideas discussed above were recently tested with graphene [14]. Atomically thin graphene cantilevers can be attached to a soft gold pad, which one can stab and move around in a water-based solvent at room temperature. Surfactants are typically needed to prevent the graphene from sticking to itself.

Free standing graphene is the ultimate 2d crystalline membrane: It is one atom thick, and at $T = 0$ has a large in-plane stiffness ($Y = 20eV/A^2$) and bending rigidity is $\kappa = 1.2eV$. Let us assume a cantilever width of $W = 10\mu$. Then, with graphene, we have reached the "Moore's Law" limit of thinness, with huge FvK numbers $\gamma \sim 10^{12}$! As mentioned above, the thermal length at room temperature is $l_{\text{th}} = 0.2$nm. Any graphene cantilever whose width exceeds this size will experience significant thermal effects [14].

One can extract the bending rigidity of graphene cantilevers by either looking at the gravitation deflection of the cantilevers or extracting the root mean square fluctuations of the end positions [14]. The bending rigdity can then be extracted by varying the cantilever length L at fixed width W. The result of such measurements is that the bending rigidity increases $\sim$3000 fold over its $T = 0$ value, consistent with renormalization group calculations $\kappa(W) \approx \kappa(W/l_{\text{th}})^\eta$ (where $\eta \approx 4/5$ and $l_{\text{th}} \approx 0.2$nm for graphene, see Figure 5.9). Additional tests of the theory could be provided by varying both temperature and the widths of the cantilevers. There may also be a contribution to the remarkable ~ 3000-fold stiffening from quenched random disorder [101].

5.6.5 Path integrals for long graphene ribbons

What about an extremely long graphene ribbon, which we can regard as an unusual, highly anisotropic polymer? The linear persistence length for a long ribbon is $l = \kappa W/k_B T$, where $W = 10\mu$ is the width of the ribbon and L is the lenght of the ribbon. This remarkable ribbon has an aspect ratio of 50,000!

Suppose we now go to scales large compared to the width of the ribbon. We can now pass to a limit where the ribbon is quasi-one-dimensional. Recall from Chapter 4 that the statistical mechanics of linear polymer chains maps onto the quantum mechanics of a quantum particle in imaginary time. As we now describe, the statistical mechanics of long ribbons maps onto the quantum mechanics of zero-dimensional rigid rotors! The free energy of a ribbon depends on the orientation of a orthonormal
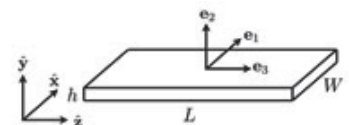

Figure 5.10: The surface of a ribbon (with height h, width W and length L) can be characterized by a triad of orthonormal vectors that vary as a function of arc length $0 \leq s \leq L$.

triad attached to the tangent plane of the ribbon, which describes the orientation of the ribbon [88],

$$F = \frac{1}{2} \int ds \left[A_1 \Omega_1^2 + A_2 \Omega_2^2 + C \Omega_3^2 \right], \tag{5.161}$$

where $\{\Omega_j\}$ is a vector of rotation angles about $\{\vec{e}_1, \vec{e}_2, \vec{e}_3\}$, which vary along the arc lengths of the ribbon $d\vec{e}_i/ds = \vec{\Omega} \times \vec{e}_i$ (see Figure 5.10). We can easily calculate the three possible derivatives of these rotations with respect to arc length,

$$\frac{d\vec{e}_j}{ds} = \vec{\Omega} \times \vec{e}_j \rightarrow \begin{cases} \left(\frac{d\vec{e}_1}{ds} \right)^2 = \Omega_2^2 + \Omega_3^2, \\ \left(\frac{d\vec{e}_2}{ds} \right)^2 = \Omega_1^2 + \Omega_3^2, \\ \left(\frac{d\vec{e}_3}{ds} \right)^2 = \Omega_1^2 + \Omega_2^2. \end{cases} \tag{5.162}$$

Eq. 5.161 can be viewed as the quantum mechanical kinetic energy of a highly anisotropic rigid rotor in imaginary time, where the arc length is a time-like variable [101].

There are various interesting limits of these results. One limit is the flexible circular limit, describing an elastic rod with circular cross section (like a wire). The angles then describe the twist and bending of the wire. Due to the circular symmetry, the bending terms simplify,

$$A_1 = A_2 = A, \quad \Omega_1^2 + \Omega_2^2 = \left(\frac{d\vec{e}_3}{ds} \right)^2, \tag{5.163}$$

and the free energy in Eq. 5.161 becomes

$$F = \frac{1}{2} \int ds \left[A \left(\frac{d\vec{e}_3}{ds} \right)^2 + C \Omega_3^2 \right]. \tag{5.164}$$

Upon integrating out the twist degrees of freedom $\Omega_3(s)$, we have a 1d Heisenberg model, with the tangent along the wire axis as the order parameter.

Another limit is an untwistable stiff belt, so the only distortion the ribbon can experience is a tilt of the normal unit vector $\vec{e}_2$. Upon taking the stiff limit,

$$A_2 = \infty, C = \infty \rightarrow \frac{d\vec{e}_1}{ds} = 0, \tag{5.165}$$

the free energy in Eq. 5.161 becomes

$$F = \frac{A_1}{2} \int ds \left(\frac{d\vec{e}_2}{ds} \right)^2, \vec{e}_2 \times \vec{e}_1 = 0 \tag{5.166}$$

which describes a 1d XY model, with an order parameter given by the normal to the untwistable belt.

The full theory, however, is much more rich and complicated [101]. As mentioned above, its statistical mechanics maps onto the path integral for a point-like quantum rotor in imaginary time. If, similar to our analysis of simpler linear polymer chains,
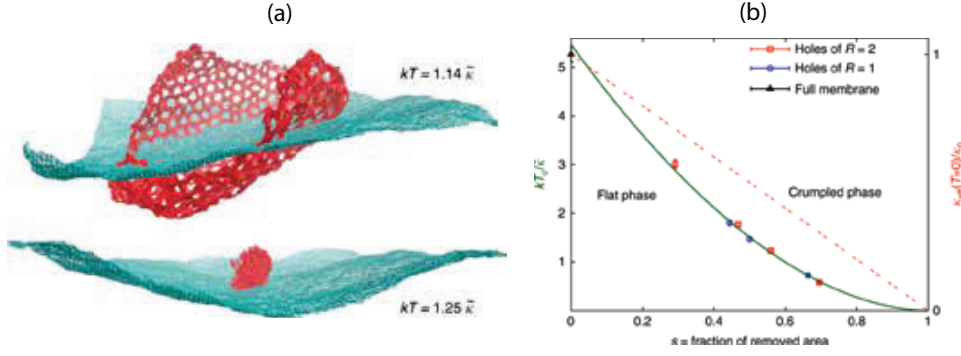
Figure 5.11: (a) Snapshots of thermalized configurations of perforated (red) and unperforated (teal) sheets. (b) Crumpling temperature $k_B T_c$ as a function of the fraction s of removed area. Figures from Ref. [84].

we subject the ribbon to a force along the z-direction, we have [88, 101],

$$E = \frac{1}{2} \int ds \left[A_1 \Omega_1^2 + A_2 \Omega_2^2 + C \Omega_3^2 \right] - Fz \tag{5.167}$$

$$A_1 = \kappa W \left(1 - \nu^2\right)/12; C = 2\kappa W (1 - \nu) \tag{5.168}$$

$$A_2 = Y W^3/12 \gg A_1, C, \tag{5.169}$$

where the last inequality reflects the parameters of a $W = 10\mu m$ graphene ribbon and ν is the Poisson ratio. The A_1 mode (bending) and C mode (twist) are both soft, but A_2 (stretching) is very large. When a force along the z-axis is added, we can map the statistical mechanics onto the quantum mechanics of a rigid rotor in an external gravitational field. For wide $W \sim 10\mu m$ graphene ribbons, one needs to use renormalized parameters such as $\kappa_R(W) \approx \kappa (W/\ell_{\text{th}})^\eta$ and $Y_R(W) \approx (\ell_{\text{th}}/W)^{\eta_u}$ in this model [101].

Can the extreme mechanics of flexural phonons be coupled to the quantum mechanics of graphene be amplified even further? One way to dramatically amplify their effects is to force the graphene to crumple, thus overcoming the diverging bending rigidity and long range order in the normals. At low temperatures, we expect a thermally wrinkled flat phase. At high enough temperature, however, a crumpling phase transition has been conjectured [79]. To estimate this temperature for graphene, recall our result for the normal-normal correlation function,

$$\langle \hat{n}(x_a) \cdot \hat{n}(x_b) \rangle \approx 1 - \frac{k_B T}{2\pi \kappa} \left[\eta^{-1} + \ln \left(\frac{\ell_{\text{th}}}{a_0} \right) \right] + C \frac{k_B T}{\kappa} \left(\frac{\ell_{\text{th}}}{|x_b - x_a|} \right)^\eta, \tag{5.170}$$

so that

$$\lim_{|x_a - x_b| \to \infty} \langle \hat{n}(x_a) \cdot \hat{n}(x_b) \rangle = |\langle \hat{n}(x) \rangle|^2 \approx 1 - \frac{k_B T}{2\pi \kappa \eta}, \tag{5.171}$$

where the last equation assumes $\ell_{\text{th}} \approx a_0$, the graphene lattice spacing. The crumpling transition temperature should be given approximately by the temperature at which $\langle n(x) \rangle$ vanishes. Unfortunately, this temperature for graphene is $T_C \approx 20000$ Kelvin, well above the temperature at which the carbon-carbon bonds of graphene fall apart! However, we could bring down this transition temperature by perforating the graphene. If we remove 80 % of the area with a regular pattern of holes [84], then the crumpling temperature can be lowered from 20000 Kelvin to 1600 Kelvin (see Figure 5.11).